

# Alzheimer's disease risk gene *BIN1* induces Tau-dependent network hyperexcitability

Yuliya Voskobiynk<sup>1†</sup>, Jonathan R Roth<sup>1†</sup>, J Nicholas Cochran<sup>1</sup>, Travis Rush<sup>1</sup>, Nancy VN Carullo<sup>2</sup>, Jacob S Mesina<sup>1</sup>, Mohammad Waqas<sup>1</sup>, Rachael M Vollmer<sup>1</sup>, Jeremy J Day<sup>2</sup>, Lori L McMahon<sup>3</sup>, Erik D Roberson<sup>1\*</sup>

<sup>1</sup>Center for Neurodegeneration and Experimental Therapeutics, Alzheimer's Disease Center, and Evelyn F. McKnight Brain Institute, Departments of Neurology and Neurobiology, University of Alabama at Birmingham, Birmingham, United States;

<sup>2</sup>Department of Neurobiology, University of Alabama at Birmingham, Birmingham, United States; <sup>3</sup>Department of Cell, Developmental and Integrative Biology, University of Alabama at Birmingham, Birmingham, United States

**Abstract** Genome-wide association studies identified the *BIN1* locus as a leading modulator of genetic risk in Alzheimer's disease (AD). One limitation in understanding *BIN1*'s contribution to AD is its unknown function in the brain. AD-associated *BIN1* variants are generally noncoding and likely change expression. Here, we determined the effects of increasing expression of the major neuronal isoform of human *BIN1* in cultured rat hippocampal neurons. Higher *BIN1* induced network hyperexcitability on multielectrode arrays, increased frequency of synaptic transmission, and elevated calcium transients, indicating that increasing *BIN1* drives greater neuronal activity. In exploring the mechanism of these effects on neuronal physiology, we found that *BIN1* interacted with L-type voltage-gated calcium channels (LVGCCs) and that *BIN1*-LVGCC interactions were modulated by Tau in rat hippocampal neurons and mouse brain. Finally, Tau reduction prevented *BIN1*-induced network hyperexcitability. These data shed light on *BIN1*'s neuronal function and suggest that it may contribute to Tau-dependent hyperexcitability in AD.

\*For correspondence: eroberson@uabmc.edu

†These authors contributed equally to this work

Competing interest: See page 19

Funding: See page 19

Received: 29 March 2020

Accepted: 12 July 2020

Published: 13 July 2020

Reviewing editor: John D Fryer, Mayo Clinic, United States

© Copyright Voskobiynk et al. This article is distributed under the terms of the [Creative Commons Attribution License](#), which permits unrestricted use and redistribution provided that the original author and source are credited.

## Introduction

Genetic discoveries have provided critical insights into potential mechanisms of Alzheimer's disease (AD), the most common neurodegenerative disease. Mutations in *APP*, *PSEN1*, or *PSEN2* cause early-onset, autosomal dominantly inherited AD, but are quite rare. Several more common genetic variants that increase AD risk to differing degrees have been identified. Among these, variants near *BIN1* have particularly high population attributable risk, because the risk allele is highly prevalent (~40% allele frequency for the index SNP, rs6733839) and has a relatively large effect size (odds ratio: 1.20; 95% confidence interval: 1.17–1.23) (Kunkle et al., 2019).

*BIN1* was first linked to AD in early genome-wide associated studies (GWAS) (Harold et al., 2009; Seshadri et al., 2010) and remains second only to *APOE* in genome-wide significance in the recent meta-analysis of 94,437 individuals by the International Genomics of Alzheimer's Disease Project (Kunkle et al., 2019). This association has been replicated in datasets with subjects from diverse genetic backgrounds (Carrasquillo et al., 2011; Hollingworth et al., 2011; Hu et al., 2011; Lambert et al., 2011; Lee et al., 2011; Logue, 2011; Naj et al., 2011; Wijsman et al., 2011; Kamboh et al., 2012; Chapuis et al., 2013; Lambert et al., 2013; Liu et al., 2013; Miyashita et al., 2013; Reitz et al., 2013; Li et al., 2015; Dong et al., 2016; Rezazadeh et al., 2016; Wang et al., 2016). Further, unbiased epigenetic analyses have provided independent evidence linking *BIN1* to

AD pathogenesis in several epigenome-wide association studies examining DNA methylation patterns in brain tissue from AD patients, in which *BIN1* again emerged as a top hit (De Jager et al., 2014; Chibnik et al., 2015; Yu et al., 2015). This association was also observed in tissue from pre-clinical AD patients, indicating that changes in *BIN1* methylation occur early in disease (De Jager et al., 2014; Chibnik et al., 2015). Also, associations between *BIN1* methylation and AD are independent of genetic variants identified in GWAS, providing an orthogonal line of evidence for *BIN1*'s involvement in AD. Importantly, *BIN1* variants have been linked to earlier age of onset (Naj et al., 2014). In addition to GWAS reports examining polymorphisms associated with AD diagnosis by clinical criteria, other studies have examined genetic risk factors for AD neuropathology. *BIN1* was significantly associated with both amyloid plaque and neurofibrillary tangle pathologies, strengthening the association with AD (Beecham et al., 2014). While these unbiased screens have convincingly implicated *BIN1* in AD pathogenesis, the mechanisms underlying the association are not yet known, and many important questions about how *BIN1* contributes to AD remain.

One of the main limitations is an incomplete understanding of *BIN1*'s normal function in the brain. Its structure suggests that a key role may involve protein trafficking at the membrane, since all *BIN1* isoforms contain an N-terminal BAR (*BIN1*/Amphiphysin/*RVS167*) domain that mediates membrane binding and curvature, plus a C-terminal SH3 domain that mediates protein–protein interactions, including with Tau (Chapuis et al., 2013; Sottejeau et al., 2015). The larger, neuron-specific isoforms also contain a clathrin-AP2 binding (CLAP) domain likely involved in endocytosis (De Rossi et al., 2016).

The *BIN1* variants associated with AD do not alter the coding sequence of *BIN1* but are rather concentrated in a presumed regulatory region upstream of the promoter. Although *BIN1* is ubiquitously expressed throughout the body, levels are highest in the brain and muscle (Butler et al., 1997), and its most critical role is in the heart, as homozygous deletion of murine *Bin1* causes early lethality due to severe ventricular cardiomyopathy (Muller et al., 2003). Canonically, *BIN1* plays a role in protein trafficking and endocytosis, specifically trafficking L-type voltage gated calcium channels (LVGCCs) in cardiac myocytes to the membrane to strengthen calcium signaling (Hong et al., 2010). However, the function *BIN1* plays in neurons remains much less clear.

In this study, we addressed *BIN1*'s role in neurons by expressing the predominant neuronal *BIN1* isoform (isoform 1) in primary hippocampal neuron cultures. Our studies revealed a role for *BIN1* in regulating neuronal activity and a potential molecular mechanism involving its interactions with calcium channel subunits.

## Results

### Higher *BIN1* induces network hyperexcitability

To begin studying the effects of altered *BIN1* levels in neurons, we first used AAV to express the predominant neuronal isoform of human *BIN1* in primary rat hippocampal neuronal cultures. We verified expression of *BIN1* using an mKate2 fluorophore fused to the C-terminus. A construct encoding mKate2 alone was used as a control. We determined that *BIN1* expression increased ~8–9-fold by immunocytochemistry and remained stable up to 3.5 weeks post transduction (Figure 1A–C). Higher *BIN1* did not change neuronal morphology (Figure 1B), the total number of neurons per well (Figure 1D–E), nor the resting membrane potential (RMP) or input resistance ( $R_{in}$ ) of cultured neurons (Table 1), indicating no significant toxic or trophic effect of overexpressing *BIN1* under these conditions.

We then recorded action potentials and burst firing in these neurons on multielectrode arrays (MEAs) after 10 days (Figure 1F–G). Local field potential (LFP) traces representing neuronal action potential and burst firing were recorded for 20 min then analyzed (Figure 1H–I). We found that higher *BIN1* levels were associated with increased frequency of action potentials (2.3-fold, Figure 1J) and action potential bursts (2.1-fold, Figure 1K). There was no change in the total number of active neurons on MEAs (Figure 1L).

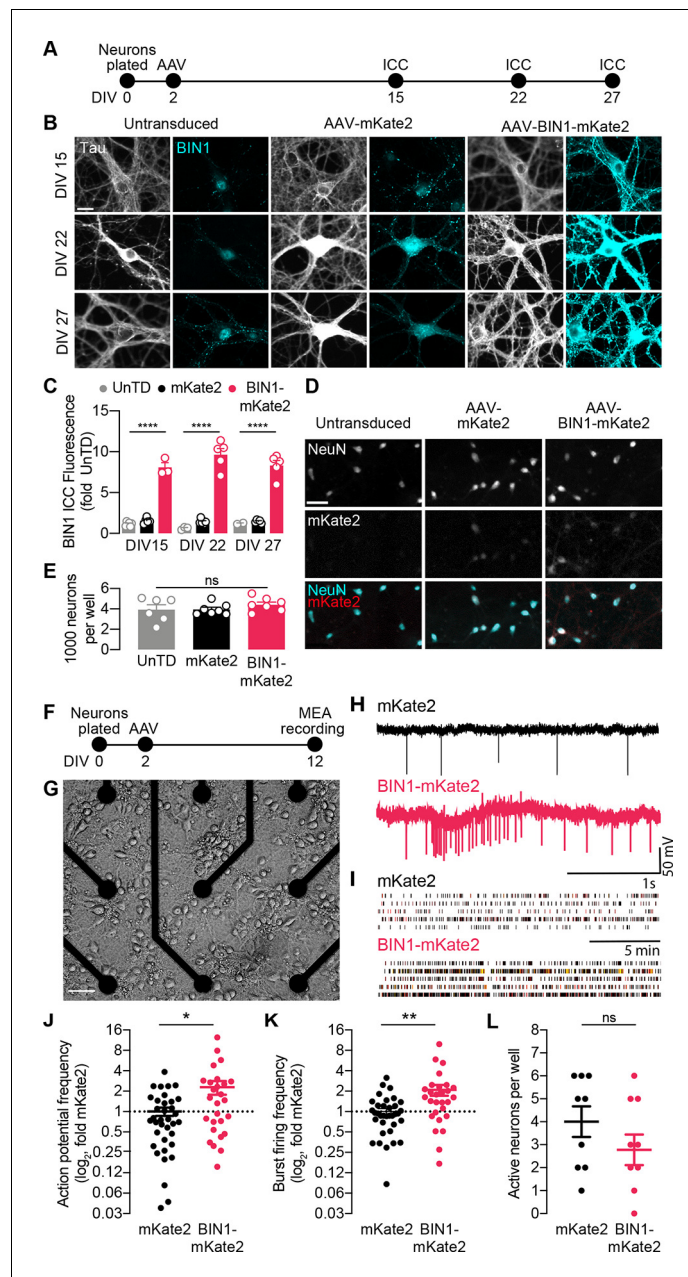


**Figure 1.** BIN1 increases action potential and burst frequency in primary hippocampal neurons cultured on microelectrode arrays (MEAs). **(A)** ICC experimental timeline: neurons were plated on day in vitro (DIV) 0, virally transduced on DIV 2, and immunostained at DIV 15, DIV 22, or DIV 27. **(B)** Representative images of primary hippocampal cultures: untransduced (left), AAV-mKate2 (center), or AAV-BIN1-mKate2 (right), showing Tau and BIN1 immunostaining at DIV 15 (top), DIV 22 (middle), or DIV 27 (bottom). Scale bar = 20  $\mu$ m. **(C)** AAV-BIN1-mKate2 increased BIN1 levels ~8–9-fold in BIN1 group compared to BIN1 levels in untransduced or mKate2 groups ( $n = 2$ –6 fields of view per coverslip, 60x magnification, two-way ANOVA, BIN-DIV interaction  $p=0.1123$ , main effect of AAV-BIN1-mKate2  $****p<0.0001$ , main effect of DIV  $p=0.6373$ , Tukey’s multiple comparisons test: DIV 15:UnTD vs. DIV 15:AAV-BIN1-mKate2,  $****p<0.0001$ , DIV 22:UnTD vs. DIV 22:AAV-BIN1-mKate2,  $****p<0.0001$ , DIV 27:UnTD vs. DIV 27:AAV-BIN1-mKate2,  $****p<0.0001$ ). **(D)** Representative images of primary hippocampal cultures at DIV 12: untransduced (left), AAV-mKate2 (center), or AAV-BIN1-mKate2 (right), showing NeuN immunostaining (top), mKate2 fluorescence (middle), or merge of both (bottom). Scale bar = 25  $\mu$ m. **(E)** The total number of neurons per well did not change between untransduced, mKate2, or BIN1 groups ( $n = 6$ –7 coverslips,  $10 \times 10$  fields of view per coverslip, 20x magnification, from two different primary neuron harvests, one-way ANOVA,  $p=0.5157$ ). **(F)** MEA experimental timeline: neurons were plated on day in vitro (DIV) 0, virally

Figure 1 continued on next page

Figure 1 continued

transduced on DIV 2, and recorded on DIV 12. (G) Primary neuronal hippocampal cultures grown on an MEA plate. Scale bar = 50  $\mu\text{m}$ . (H) Representative local field potential (LFP) traces. (I) Representative raster plots of firing activity from five different neurons per group. (J) BIN1 increased action potential frequency ( $n = 27\text{--}36$  neurons per group from three different primary neuron harvests, normalized to the controls from each harvest, median frequency in controls = 388 mHz; unpaired Mann-Whitney U test;  $p=0.0233$ ). (K) BIN1 increased burst firing frequency ( $n = 27\text{--}36$  neurons per group from three different primary neuron harvests, normalized to the controls from each harvest, median frequency in controls = 11.7 mHz; unpaired Mann-Whitney U test;  $p=0.0020$ ). (L) The total number of active neurons per well did not differ between mKate2 and BIN1 expressing groups ( $n = 9$  MEA plates for each group from three different primary neuron harvests, unpaired Student's t test;  $p=0.346$ ). All data are expressed as mean  $\pm$  SEM, \* $p<0.05$ , \*\* $p<0.01$ , and \*\*\*\* $p<0.0001$ . All data are expressed as mean  $\pm$  SEM.

## Higher BIN1 increases frequency of spontaneous excitatory and inhibitory synaptic transmission

Since higher BIN1 levels increased action potential and burst frequencies in the MEA recordings, we hypothesized that this would be associated with an increased frequency of spontaneous excitatory postsynaptic currents (sEPSCs). To test this, we used whole-cell voltage-clamp recordings from BIN1-transduced neurons at DIV 19–21 (Figure 2A), pharmacologically isolating sEPSCs using picrotoxin to block inhibitory GABA<sub>A</sub>R currents (Figure 2B). Consistent with the increased action potential frequency observed in MEA recordings (Figure 1E), higher BIN1 levels were associated with dramatically increased sEPSC frequency (interevent interval decreased >50%) (Figure 2C). sEPSC amplitudes differed by <10% (Figure 2D).

To investigate if this effect of higher BIN1 levels was selective for excitatory transmission, we next examined whether higher BIN1 expression had similar effects on spontaneous inhibitory postsynaptic currents (sIPSCs). We determined the proportion of GABAergic interneurons in our primary hippocampal cultures and found that 10% of the neurons were GAD67 positive (Figure 2E), consistent with prior work (Benson et al., 1994). To determine the effect of higher BIN1 levels on inhibitory synaptic transmission from these neurons, we recorded pharmacologically isolated GABA<sub>A</sub>R-mediated sIPSCs using DNQX, APV, and nifedipine to block AMPARs, NMDARs, and L-type voltage-gated calcium channels (LVGCCs), respectively (Figure 2F). Similar to the effect on sEPSC frequency, higher BIN1 increased sIPSC frequency (decrease in interevent interval, Figure 2G). There was a coincident decrease in sIPSC amplitude (Figure 2H).

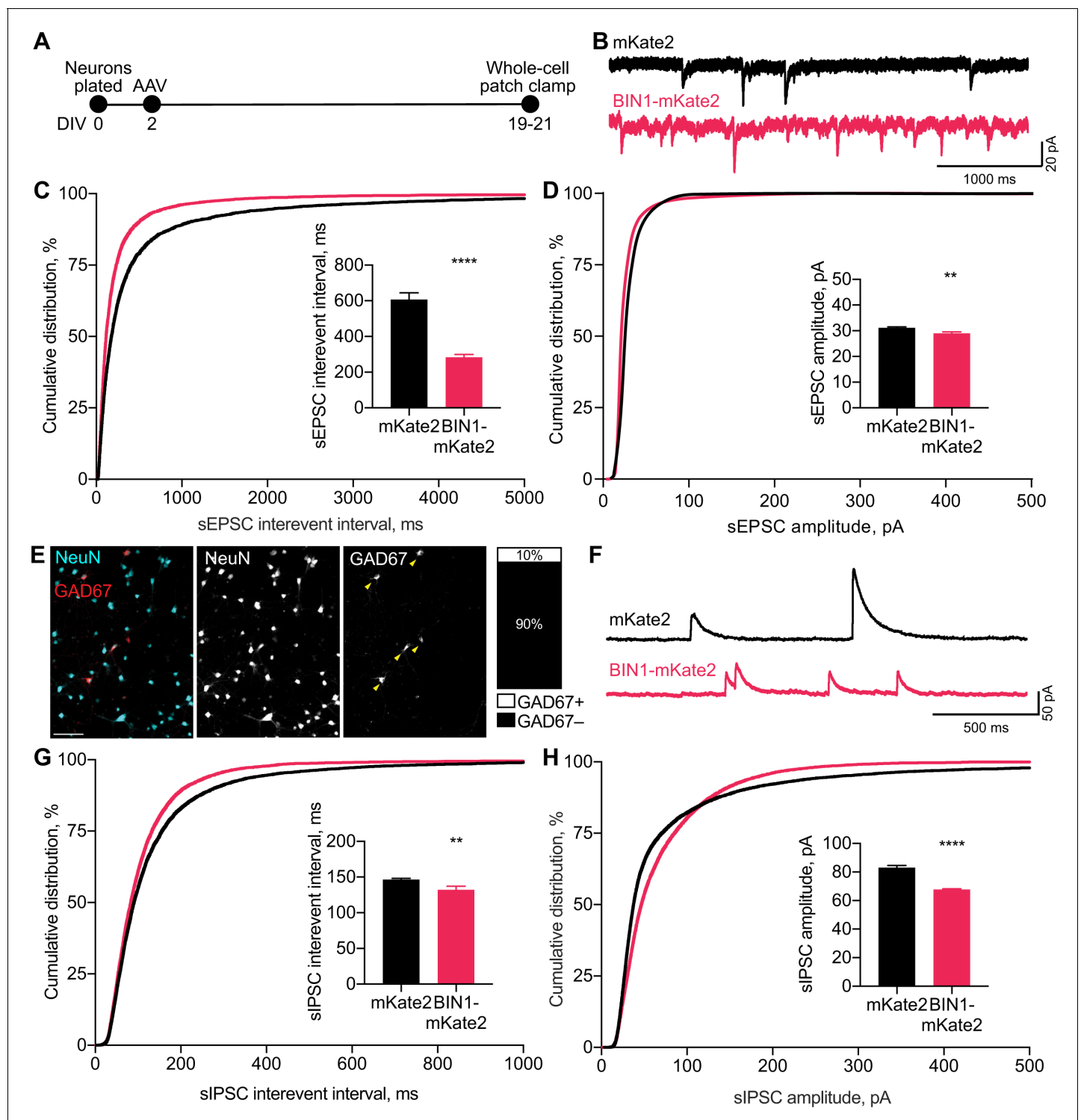
Overall, these findings suggest that higher BIN1 levels increase the frequency of both sEPSCs and sIPSCs in primary hippocampal cultures, agreeing with the increased action potential firing observed using MEAs (Figure 1E–F).

## Higher BIN1 in mature neurons increases calcium influx

Using AAVs requires transduction soon after plating (DIV 2) because of the time required for transgene expression, so some effects could be due to increasing BIN1 levels during early neuronal development. To dissociate the effect of higher BIN1 on network hyperexcitability from neuronal development, we transiently transfected primary hippocampal cultures at DIV 14, when neurons are more fully developed (Figure 3A). We co-transfected BIN1 constructs with the genetically encoded calcium indicator, GCaMP6f, which allows for single neuron calcium imaging in primary hippocampal cultures. We used two BIN1 constructs, both based on human isoform one tagged with the mKate2

**Table 1.** Resting membrane potential (RMP) and input resistance ( $R_{in}$ ) in patched hippocampal neurons did not differ across untransduced, AAV-mKate2, and AAV-BIN1-mKate2 groups.

	RMP, mV	$R_{in}$ , M $\Omega$	N, Cells
Untransduced	$-60.43 \pm 5.36$	$843.04 \pm 55.11$	4
AAV-mKate2	$-59.90 \pm 3.70$	$834.83 \pm 41.09$	6
AAV-BIN1-mKate2	$-62.40 \pm 2.24$	$790.18 \pm 15.74$	7
One-way ANOVA, $p$	0.85	0.36	



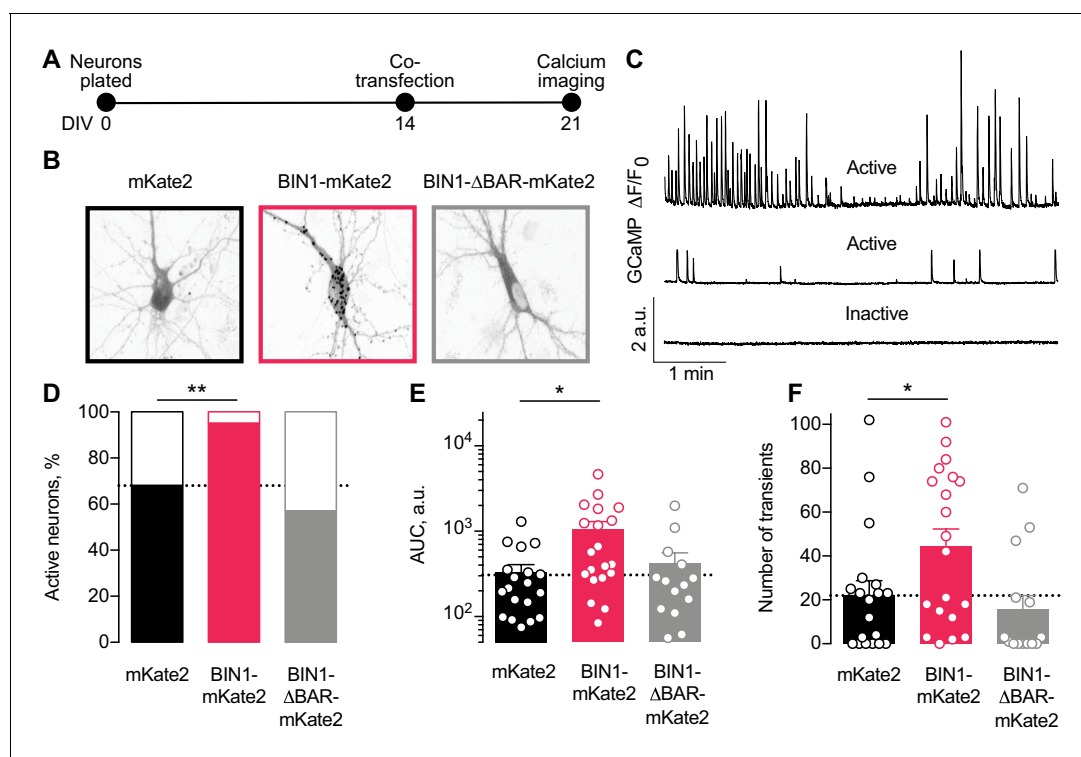
**Figure 2.** BIN1 increases both excitatory and inhibitory synaptic transmission. (A) Synaptic transmission recordings experimental timeline: neurons were plated on DIV 0, virally transduced on DIV 2, electrophysiologically recorded on DIV 19–21. (B) Representative traces of sEPSCs recorded from neurons transduced with mKate2 or BIN1. (C) BIN1 decreased mean sEPSC interevent interval (Kolmogorov-Smirnov test on cumulative distribution, \*\*\*\* $p < 0.0001$ , KS D score: 0.1657; unpaired two-tailed Student's t-test on mean IEI, \*\*\*\* $p < 0.0001$ ). (D) BIN1 slightly decreased mean sEPSC amplitude unpaired (Kolmogorov-Smirnov test on cumulative distribution, \*\*\*\* $p < 0.0001$ , KS D score: 0.1803; unpaired two-tailed Student's t-test on mean amplitude, \*\*\* $p = 0.0004$ ) ( $n = 12$ – $21$  neurons per group from three different primary neuron harvests). (E) Representative images and quantification of NeuN and GAD67+ neurons in primary hippocampal cultures at DIV 12 ( $n = 255$  GAD67+ neurons,  $n = 2342$  NeuN+ neurons, from 10 randomly taken images per coverslip, 10 coverslips from two different primary neuron harvests.) Scale bar = 100  $\mu\text{m}$ . (F) Representative traces of sIPSCs recorded from Figure 2 continued on next page

Figure 2 continued

neurons transduced with mKate2 or BIN1. (G) BIN1 decreased mean sIPSC interevent interval (Kolmogorov-Smirnov test on cumulative distribution, \*\*\*\* $p < 0.0001$ , KS D score: 0.06862; unpaired two-tailed Student's t-test on mean IEI, \*\* $p = 0.0035$ ) (H) BIN1 decreased mean sIPSC amplitude (Kolmogorov-Smirnov test on cumulative distribution, \*\*\*\* $p < 0.0001$ , KS D score: 0.1297; unpaired two-tailed Student's t-test on mean amplitude, \*\*\*\* $p < 0.0001$ ) ( $n = 11$ – $16$  neurons per group from three different primary neuron harvests). All data are expressed as mean  $\pm$  SEM.

fluorophore. In addition to the full-length BIN1 construct used in **Figures 1–2**, we also used a construct engineered to remove the BAR domain ( $\Delta$ BAR), which is predicted to abolish BIN1 membrane localization, and thus likely its activity. As before, mKate2 alone was used as a control construct. Interestingly, the pattern of mKate2 distribution within the neurons was strikingly different across groups, as mKate2 and BIN1- $\Delta$ BAR exhibited diffuse localization throughout the soma, neurites, and nucleus, while wild-type BIN1 had a punctate distribution throughout the cytosol but was excluded from the nucleus (**Figure 3B**). These observations agree with BAR-domain dependent membrane localization of BIN1 found in other cell types (**Hong et al., 2010; Picas et al., 2014**).

We monitored basal calcium activity of individual transfected neurons by imaging GCaMP fluorescence using laser scanning microscopy. We measured the change in somatic GCaMP fluorescence intensity relative to the quiescent period between transients (defined as  $F_0$ ) and classified neurons as either active ( $\geq 1$  calcium transient) or inactive (no calcium transients) (**Figure 3C**).



**Figure 3.** Higher BIN1 levels in mature neurons increase calcium influx in primary hippocampal neuronal cultures. (A) Calcium imaging experimental timeline: neurons were plated on DIV 0, co-transfected on DIV 14 with GCaMP6f calcium indicator and either BIN1-mKate2, BIN1- $\Delta$ BAR-mKate2, or mKate2 control construct, and recorded on DIV 21.  $n = 14$ – $20$  neurons per condition. (B) mKate2 fluorescence in primary transfected primary hippocampal neurons. BIN1-mKate2 fluorescence was punctate in transfected neurons. mKate2 and BIN1- $\Delta$ BAR-mKate2 fluorescence was diffuse and filled the neuron. (C) GCaMP fluorescence intensity,  $F$ , relative to the quiescent period between transients,  $F_0$ . Neurons were classified as either active (with a range of activity levels indicated by the top and middle traces) or inactive (no calcium transients during the 8 min recording, bottom trace). (D) BIN1, but not BIN1- $\Delta$ BAR, increased the proportion of active neurons (Binomial test, \*\* $p = 0.0071$ ). (E) BIN1, but not BIN1- $\Delta$ BAR, increased neuronal calcium influx measured as area under the curve (AUC; one-way ANOVA,  $p = 0.0134$ ; Dunnett's posthoc, \* $p = 0.0122$ ). (F) BIN1, but not BIN1- $\Delta$ BAR, increased the number of calcium transients (one-way ANOVA,  $p = 0.0144$ ; Dunnett's posthoc, mKate2 vs BIN1-mKate2 adjusted \* $p = 0.0437$ ). All data are expressed as mean  $\pm$  SEM.

About a third of neurons were inactive under control conditions (**Figure 3D**), consistent with prior studies (*Kuijlaars et al., 2016; Lerdkrai et al., 2018*). However, neurons expressing the full-length human BIN1 construct were almost never inactive (**Figure 3D**). As expected, the BIN1- $\Delta$ BAR construct was similar to controls (**Figure 3D**), indicating the importance of BIN1 membrane localization for the effect. Increasing BIN1 levels roughly doubled calcium influx as measured by both area under the curve (**Figure 3E**) and the number of calcium transients (**Figure 3F**).

### BIN1 interacts with LVGCCs in neurons

We were interested to find that the ability of BIN1 to increase neuronal activity was dependent on the presence of the BAR domain, which is critical for its membrane localization. One of BIN1's known functions outside of the brain is localizing LVGCCs to the membrane of cardiomyocyte T-tubules (*Hong et al., 2010; Hong et al., 2014*). Therefore, we asked if BIN1 interacts with LVGCCs in neurons and if increased interaction between BIN1 and LVGCCs could be a potential mechanism by which BIN1 increases neuronal activity.

To begin addressing this question, we first examined BIN1 interactions with LVGCC beta-1 subunits (LVGCC- $\beta$ 1), which reside on the inner face of the membrane and target LVGCCs to the membrane (*Buraei and Yang, 2010*). To determine whether BIN1 and LVGCC- $\beta$ 1 interact directly, we used proximity ligation assay (PLA), which allows quantification and visualization of protein-protein interactions in situ, producing a fluorescent punctum whenever the two antibody epitopes are within 40 nm (i.e., directly interacting or nearby in a complex). We detected endogenous BIN1–LVGCC- $\beta$ 1 interaction in neuronal soma and neurites of untransduced neurons (**Figure 4A**). If a BIN1-mediated effect on LVGCC's underlies the observed effects on neuronal activity, then AAV-BIN1 constructs should increase the interaction (**Figure 4B**). Transduction with BIN1-mKate2 substantially increased BIN1–LVGCC- $\beta$ 1 interaction, while transduction with the mKate2 control vector did not change endogenous interaction levels (**Figure 4C,D**).

### BIN1-LVGCC interaction is Tau-dependent

Multiple studies have demonstrated that BIN1 directly interacts with Tau, both in vitro and in vivo (*Chapuis et al., 2013; Lasorsa et al., 2018; Sartori et al., 2019*). This interaction between BIN1 and Tau is mediated by the SH3 domain of BIN1 and PxxP motifs in Tau's central proline-rich region. Interestingly, LVGCC- $\beta$ 1 also harbors an SH3 domain that could also interact with Tau. Thus, we hypothesized that the BIN1 interaction with LVGCC- $\beta$ 1 might be at least in part scaffolded by Tau (**Figure 5A**).

We first used a live-cell bioluminescence resonance energy transfer (BRET) assay (*Cochran et al., 2014*) to determine if Tau interacts with the SH3 domains of both BIN1 and LVGCC- $\beta$ 1. We transfected CHO cells with Tau-mKate2 (acceptor) and either the BIN1 SH3 domain or LVGCC- $\beta$ 1 SH3 domain tagged with click beetle green (donor) (**Figure 5B**). Both Tau–BIN1 and Tau–LVGCC- $\beta$ 1 demonstrated BRET, indicating that Tau interacts with each of these SH3 domains (**Figure 5C**).

We then tested the hypothesis that Tau affects the BIN1–LVGCC $\beta$ 1 interaction, using the BIN1–LVGCC- $\beta$ 1 PLA assay with and without pretreatment with Tau antisense oligonucleotide (ASO) (**Figure 5D**). We recently demonstrated that this ASO reduces Tau protein by about 50% under these conditions (*Rush et al., 2020*). Tau reduction decreased BIN1–LVGCC- $\beta$ 1 interaction in primary hippocampal neurons, compared to neurons treated with a scrambled control ASO (**Figure 5E**), indicating that in cultured neurons the BIN1–LVGCC- $\beta$ 1 interaction is partially Tau-dependent.

Next, we determined if the BIN1–LVGCC- $\beta$ 1 interaction is also Tau-dependent in vivo. Using cortical brain lysates from wild-type and Tau knockout (Tau KO) mice, we immunoprecipitated LVGCC- $\beta$ 1 and blotted for BIN1. BIN1 co-immunoprecipitated with LVGCC- $\beta$ 1 from these brain lysates, and the BIN1–LVGCC- $\beta$ 1 complex was reduced in Tau KO brains, without any difference in LVGCC- $\beta$ 1 immunoprecipitation (**Figure 5F**). Taken together, these data indicate that the BIN1–LVGCC interaction is partially Tau-dependent both in vitro and in vivo.

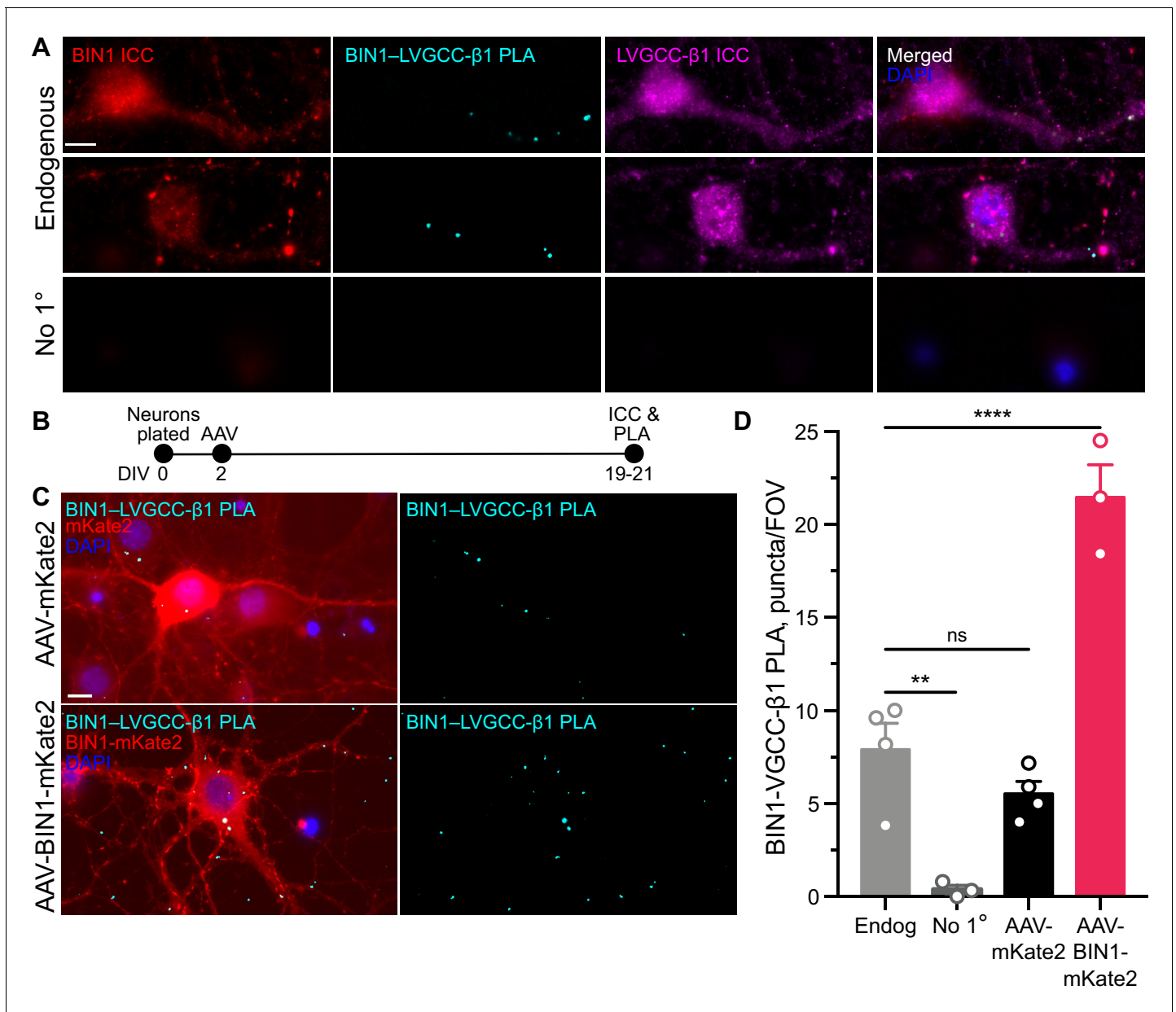


**Figure 4.** BIN1 interacts with LVGCC- $\beta$ 1 subunits in neurons. (A) Localization of endogenous BIN1, LVGCC- $\beta$ 1, and endogenous BIN1-LVGCC- $\beta$ 1 interaction detected by PLA. Scale bar = 10  $\mu$ m. (B) Experimental timeline: neurons were plated on DIV 0, transduced with AAV-BIN1-mKate2 or AAV-mKate2 on DIV 2, and fixed and stained on DIV 19–21. (C) Representative images of mKate2 fluorescence, BIN1-LVGCC- $\beta$ 1 PLA puncta, and BIN1 ICC in primary hippocampal neurons. Scale bar = 10  $\mu$ m. (D) BIN1-LVGCC- $\beta$ 1 interaction was increased by BIN1 ( $n = 3$ –4 coverslips per group, each with 5 fields of view averaged, from three different primary neurons harvests; one-way ANOVA,  $p < 0.0001$ ; Endogenous vs. AAV-BIN1-mKate2 \*\*\*\* $p = 0.0001$  by Dunnett’s post-hoc). All data are expressed as mean  $\pm$  SEM.

## Tau reduction prevents network hyperexcitability induced by higher BIN1

Tau reduction is protective in many models of AD and it reduces network hyperexcitability in many disease models, including AD and epilepsy models (Chin et al., 2007; Roberson et al., 2007; Holth et al., 2011; Roberson et al., 2011; DeVos et al., 2013; Gheyara et al., 2014; Liu et al., 2017). Thus, since Tau reduction decreases BIN1-LVGCC- $\beta$ 1 interaction in primary hippocampal neurons and brain homogenates, we asked whether Tau reduction attenuates network hyperexcitability induced by increased BIN1.



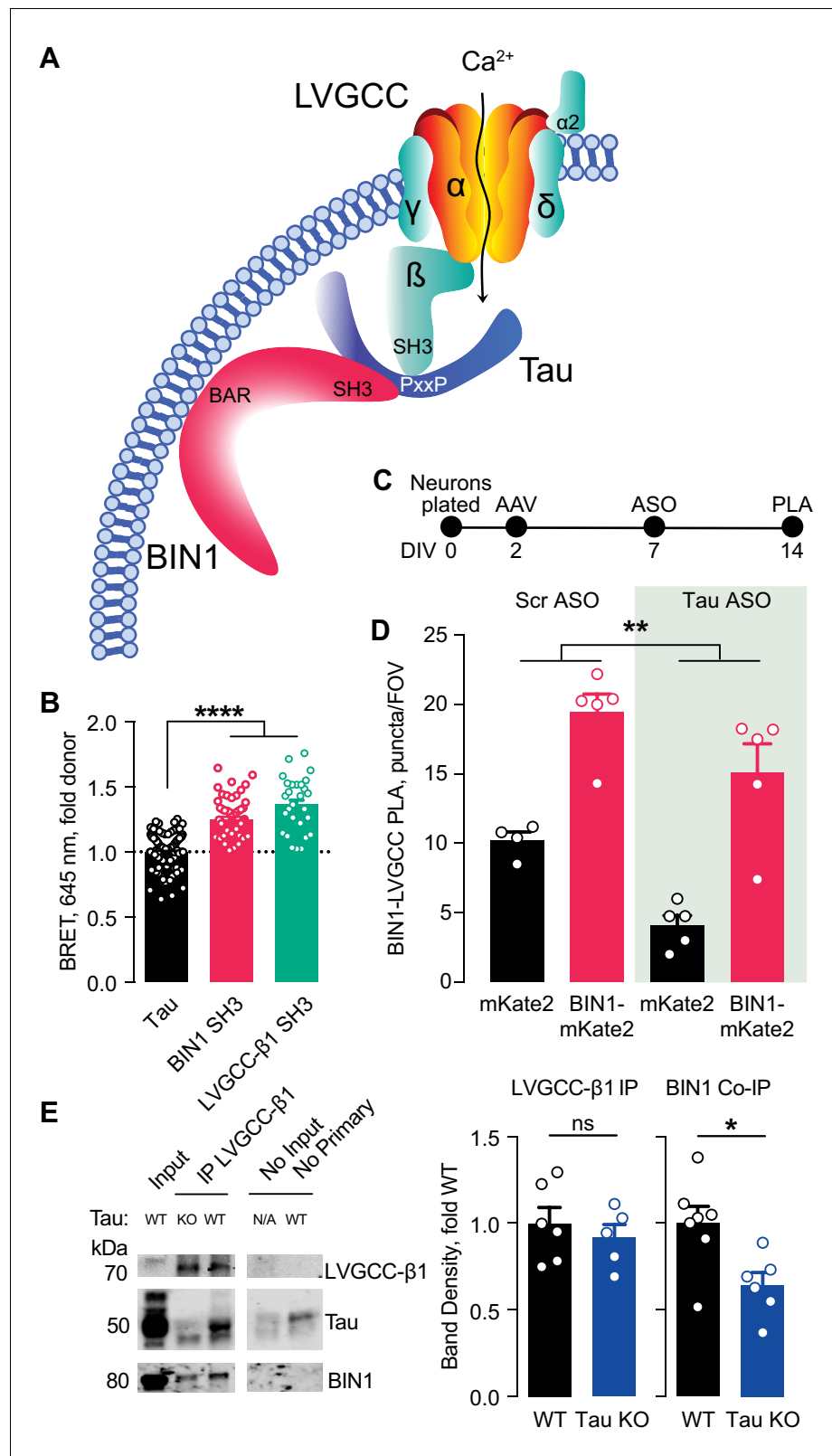


**Figure 5.** Tau-dependent BIN1-LVGCC interaction. (A) Model of Tau-dependent BIN1-LVGCC interaction. BIN1's BAR domain localizes BIN1 to the plasma membrane, and PxxP motifs in Tau's central proline-rich domain interact with the SH3 domains of BIN1 and LVGCC-β1. (B) Tau interacts with both BIN1 and LVGCC-β1 SH3 domains detected by bioluminescence resonance energy transfer (BRET) (n = 28–164 wells, one-way ANOVA, Figure 5 continued on next page

Figure 5 continued

\*\*\*\* $p < 0.0001$ ). (C) Experimental timeline of BIN1–LVGCC- $\beta 1$  PLA: neurons were plated on DIV 0, transduced with AAV-BIN1-mKate2 or AAV-mKate2 on DIV 2, treated with Tau or scrambled ASO on DIV 7, and stained on DIV 14. (D) AAV-BIN1-mKate2 increased BIN1–LVGCC- $\beta 1$  interaction, while Tau reduction with Tau ASO decreased BIN1–LVGCC- $\beta 1$  interactions ( $n = 4–6$  coverslips per group representing an average of 4–5 fields of view (FOV) per coverslip from three different neuronal harvests; Two-way ANOVA, main effect of Tau ASO \*\* $p = 0.0018$ , main effect of AAV-BIN1-mKate2 \*\*\*\* $p < 0.0001$ ). (E) We immunoprecipitated LVGCC- $\beta 1$  followed by western blotting for LVGCC- $\beta 1$ , Tau, and BIN1 from cortical homogenates of wild-type and Tau KO mice. The amount of LVGCC- $\beta 1$  immunoprecipitated did not differ between wild-type and Tau KO brains ( $n = 5–6$  mice, 3.56  $\pm$  0.04 months old, unpaired Student's  $t$  test;  $p = 0.5105$ ). However, the amount of BIN1 co-immunoprecipitated with LVGCC- $\beta 1$  was decreased in Tau KO brains compared to wild-type litter mate controls ( $n = 5–6$  mice, unpaired Student's  $t$  test; \* $p = 0.0157$ ). All data are expressed as mean  $\pm$  SEM.

To do this, we utilized a 48-well MEA system to permit recordings from many neurons with in-plate controls for each experiment. We grew neurons on the MEA, transduced them with AAV-BIN1 or AAV-mKate2 control, applied Tau ASO or a scrambled ASO control, then recorded neuronal activity (Figure 6A). As in our initial experiments, these manipulations did not affect the number of active neurons (Figure 6B), and higher BIN1 levels increased neuronal firing in this system as well (Figure 6C–D). Tau reduction completely blocked the BIN1-induced increases in action potential frequency (Figure 6E–F) and bursting (Figure 6G–H). These results demonstrate that BIN1-induced network hyperexcitability is Tau-dependent and add to the body of work demonstrating beneficial effects of Tau reduction on limiting network hyperexcitability and AD-related dysfunction.

## Discussion

Genetic data indicate that BIN1 can play an important role in AD pathogenesis, but a major limitation is the relatively poor understanding of BIN1's function in the central nervous system. We found that expressing the predominant human BIN1 isoform in primary hippocampal cultures led to a Tau-dependent increase in neuronal activity leading to network hyperexcitability. Higher BIN1 levels increased the frequency of both spikes and bursts recorded with multielectrode arrays (Figure 1). Using patch-clamp recordings of neurons overexpressing BIN1, we observed increased frequency of both excitatory and inhibitory synaptic transmission (Figure 2). Similarly, elevating BIN1 levels also increased calcium spikes in neurons co-transfected with the calcium indicator GCaMP6f (Figure 3). To understand the potential mechanism of increased calcium influx, we explored potential interactions with LVGCCs, which contribute to BIN1 effects on cardiac excitability. BIN1 interacted with LVGCCs in neurons in a Tau-dependent manner, assessed by both proximity ligation assay in cultured neurons and co-immunoprecipitation from brain (Figures 4–5). Finally, using a high-content multielectrode array system, we showed that Tau reduction prevented network hyperexcitability induced by BIN1 (Figure 6). Together, these data show Tau-dependent regulation of neuronal activity by the Alzheimer's disease risk gene *BIN1* and generate new insights about the mechanistic role BIN1 may play in AD.

Increasing evidence supports the idea that changes in neuronal excitability may contribute to AD pathogenesis. Functional imaging studies reveal hyperactivation of many brain regions in AD patients (Dickerson et al., 2005; Hämäläinen et al., 2007). This is an early event in AD pathogenesis, seen in asymptomatic individuals at genetic risk for AD (Bookheimer et al., 2000; Reiman et al., 2012). In addition, childhood epilepsy can drive subsequent amyloid accumulation (Joutsa et al., 2017). Furthermore, seizures are more frequent in AD patients than in age-matched controls (Amatniek et al., 2006; Palop and Mucke, 2009; Scarneas et al., 2009), and in the early stages of disease, even patients without overt seizures often have epileptiform activity on neurophysiological recordings (Vossel et al., 2013; Vossel et al., 2016). Even more importantly, late-onset unprovoked seizures in older veterans are associated with a 2-fold risk of developing dementia, likely a first sign of neurodegenerative disease (Keret et al., 2020). Hyperexcitability is also seen in mouse models of AD, many of which have seizures (often nonconvulsive) and epileptiform spikes (Palop et al., 2007; Minkeviciene et al., 2009), excitation-inhibition imbalance in synaptic recordings (Roberson et al., 2011), and increased intrinsic neuronal excitability (Brown et al., 2011).

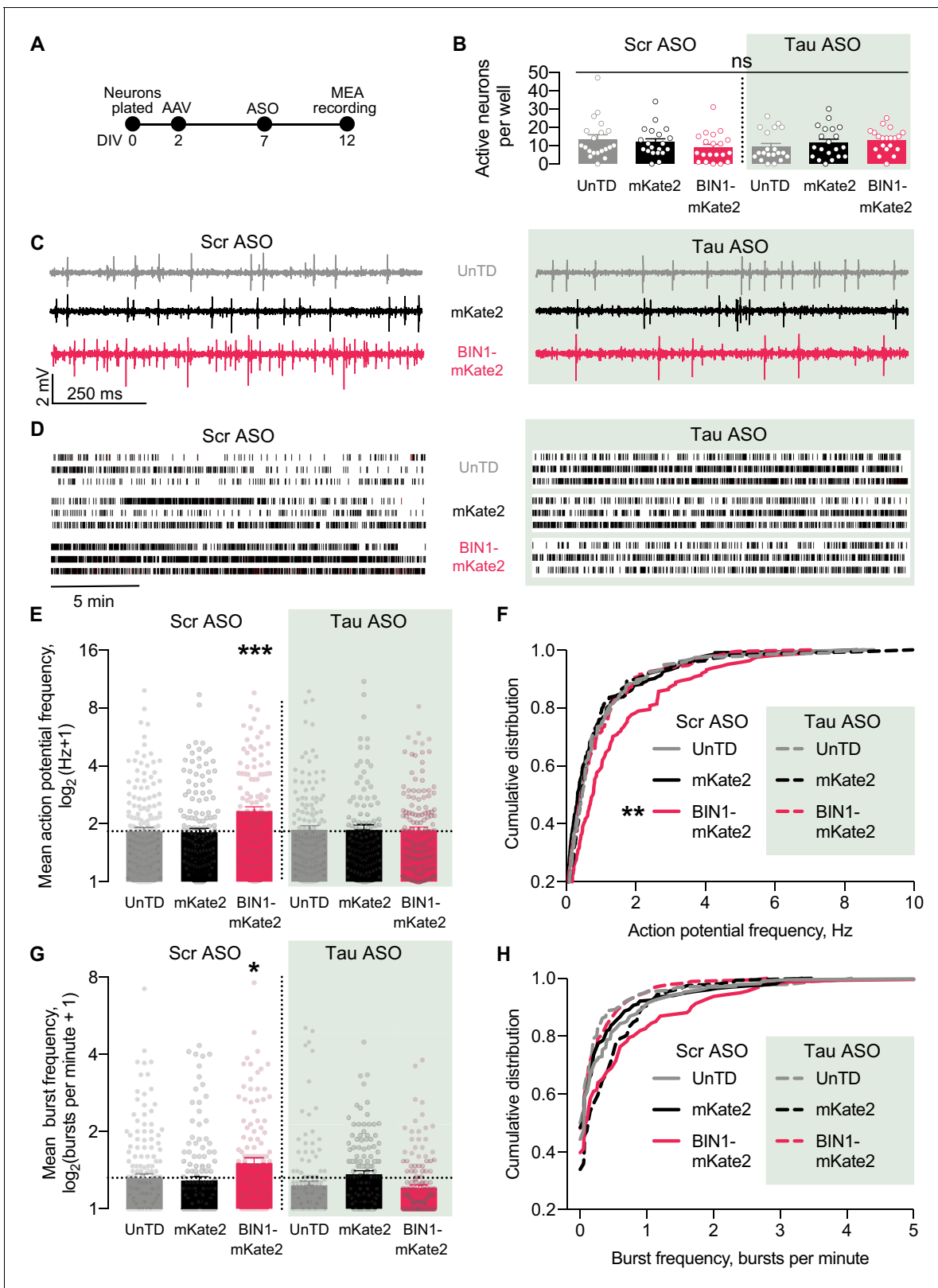


**Figure 6.** Tau reduction prevents network hyperexcitability induced by BIN1. (A) MEA experimental timeline: neurons were plated on DIV 0, virally transduced on DIV 2, treated with Tau or scrambled ASO on DIV 5, and electrophysiologically recorded on DIV 12. (B) The number of active neurons was not different between groups ( $n = 6-8$  coverslips per group from three different neuronal harvests; two-way ANOVA, main effect of Tau ASO  $p=0.9140$ , main effect of AAV-BIN1-mKate2  $p=0.9026$ , interaction  $p=0.1101$ ). (C) Representative LFP traces of MEA recordings. (D) Representative raster plots. Figure 6 continued on next page

Figure 6 continued

plots of MEA recordings. (E) Tau reduction prevented BIN1-induced network hyperexcitability as measured by mean action potential frequency ( $n = 159\text{--}230$  neurons from 6 to 8 wells per group from three different neuronal harvests; two-way ANOVA, BIN-Tau interaction  $**p=0.0073$ , main effect of Tau ASO  $p=0.0761$ , main effect of AAV-BIN1-mKate2  $*p=0.0130$ , Sidak's multiple comparisons test: UnTd:Scr ASO vs. BIN1-mKate2:Scr ASO  $***p=0.0010$ ). (F) Cumulative distribution of the mean action potential frequency (Kolmogorov-Smirnov test on cumulative distribution, UnTD-Scr ASO vs. BIN1-mKate2-Scr ASO  $**p=0.0028$ ). (G) Tau reduction prevented BIN1-induced network hyperexcitability as measured by mean burst frequency ( $n = 159\text{--}230$  neurons from 6 to 8 wells per group from three different neuronal harvests; two-way ANOVA, BIN-Tau interaction  $***p=0.0005$ , main effect of Tau ASO  $**p=0.0066$ , main effect of AAV-BIN1-mKate2  $p=0.2286$ , Sidak's multiple comparisons test: UnTd:Scr ASO vs. BIN1-mKate2:Scr ASO  $*p=0.0227$ ). (H) Cumulative distribution of the burst frequency (Kolmogorov-Smirnov test on cumulative distribution, UnTD-Scr ASO vs. BIN1-mKate2-Scr ASO,  $p=0.1107$ ). All data are expressed as mean  $\pm$  SEM.

Existing data are consistent with a potential role for BIN1 in controlling neuronal excitability. As a membrane scaffolding protein, BIN1 promotes T-tubule formation in skeletal muscles (Tjondrokoesoemo et al., 2011). In cardiomyocytes, Bin1 traffics LVGCCs to T-tubules, allowing for proper T-tubule formation and excitation-contraction coupling (Hong et al., 2010; Hong et al., 2014). Genetic loss of Bin1 in cardiomyocytes decreases surface localization of LVGCCs to T-tubules and decreases LVGCC calcium transients (Hong et al., 2010). In addition, acute knockdown of Bin1 in primary cortical neurons reduced calcium spikes in response to NMDA (McAvoy et al., 2019). Similarly, a chronic genetic deletion of Bin1 in mice decreased mEPSCs frequency, suggesting an effect of Bin1 on synaptic transmission (De Rossi et al., 2020). Complementary to these studies on effects of decreased Bin1 expression in mice, we found that increased human BIN1 expression increases synaptic transmission, neuronal activity, and calcium transients, and that BIN1 interacts with LVGCCs in neurons. Moreover, we found that higher BIN1 increases not only excitatory, but also inhibitory synaptic transmission. Human genetics also support a link between BIN1 and network hyperexcitability, as the risk allele of the rs744373 variant upstream of *BIN1*, which is linked to AD, is also associated with impaired memory in temporal lobe epilepsy patients (Bungenberg et al., 2016).

Further studies will be needed to elucidate the precise mechanisms by which BIN1 regulates neuronal firing, but our studies suggest an effect on surface trafficking of LVGCCs. While biophysical and pharmacological properties of LVGCCs are tightly controlled by the principal  $\alpha 1$  subunit, the cytosolic auxiliary  $\beta$  subunit plays an essential role in trafficking of LVGCCs to the plasma membrane (Buraei and Yang, 2010). Our study revealed BIN1 interaction with these LVGCC  $\beta$  subunits in neurons (Figures 4–5), likely contributing to LVGCC neuronal surface localization. LVGCCs modulate neuronal firing (Liu et al., 2014) and control both basal and bursting neuronal activity through somatic and dendritic  $\text{Ca}^{2+}$  transients (Morton et al., 2013; Liu et al., 2014). LVGCCs are also linked to neurodegeneration by carrying toxic amounts of  $\text{Ca}^{2+}$  through an increase of LVGCC activity, density, or exposure to  $\beta$ -amyloid peptides (Cataldi, 2013).

Our findings suggest that the effects of BIN1 on neuronal excitability likely involve Tau. A variety of evidence has linked BIN1 to Tau in studies of AD. In AD patients, the *BIN1* risk variant, rs744373, is associated with increased Tau-PET levels, as well as reduced functional connectivity and impaired memory (Zhang et al., 2015; Franzmeier et al., 2019). The fact that BIN1 localizes in a complex with Tau (Figures 4–5; Chapuis et al., 2013; Zhou et al., 2014; Sottejeau et al., 2015; Bretteville et al., 2017; Malki et al., 2017; Lasorsa et al., 2018) supports the hypothesis that BIN1–Tau interaction regulates neuronal excitability, as there is now abundant data that a key function of Tau is regulating neuronal excitability, particularly susceptibility to hyperexcitability. This includes the fact that Tau<sup>+/-</sup> and Tau<sup>-/-</sup> mice are resistant to epileptiform activity and seizures induced by excitotoxic agents (Roberson et al., 2007; Ittner et al., 2010; Roberson et al., 2011). Tau knockdown using ASOs also has excitoprotective effects against hyperexcitability in mice (DeVos et al., 2013), complemented by our finding of excitoprotective effects against BIN1-induced hyperexcitability (Figure 6).

The precise effects of AD-associated *BIN1* variants remains to be fully understood, but their effects are likely to be mediated through changes in expression levels since they do not affect the coding sequence. For example, the risk allele of the AD-associated rs744373 variant drives increased expression of BIN1 (Bungenberg et al., 2016). While another early report suggested increased BIN1 in AD (Chapuis et al., 2013), subsequent reports suggest that variants may reduce BIN1 expression

(Glennon *et al.*, 2013; Holler *et al.*, 2014), and the effects may also differ between the neuronal and ubiquitous isoforms (De Rossi *et al.*, 2016). Ongoing studies will provide additional evidence about the directionality of *BIN1* variant effects on expression, but our findings are consistent with either increases or decreases in *BIN1* contributing to network hyperexcitability in AD, since we found that higher *BIN1* was associated with higher activity as a general effect in both excitatory and inhibitory neurons. That is, either increased *BIN1* in excitatory neurons with corresponding increased excitatory activity, or reduced *BIN1* in inhibitory neurons with corresponding reduced inhibition, could lead to network hyperexcitability. Further study will be required to better understand both the effects of AD-associated *BIN1* variants and the relative balance between excitatory and inhibitory neuron effects of *BIN1*. In addition, *BIN1* expression changes in oligodendrocytes or microglia also warrant study for their potential roles in AD (De Rossi *et al.*, 2016; Nott *et al.*, 2019).

Our findings highlight the potential importance of Tau interactions with SH3 domain-containing proteins. We recently demonstrated that inhibiting Tau-SH3 interactions can reduce A $\beta$  toxicity (Rush *et al.*, 2020), and it is notable that *BIN1* joins a growing list of SH3 domain-containing proteins that interact with Tau and are implicated in AD. Tau may act as a scaffolding protein through *BIN1* interactions mediating membrane localization (Figure 5A), promoting network hyperexcitability through its SH3-domain containing binding partners. This could be a critical role for Tau and explain how mislocalization of Tau in AD contributes to the increased network excitability seen in AD pathogenesis. This would be consistent with the finding that reducing endogenous Tau prevents network hyperexcitability and A $\beta$ -induced dysfunction in AD models.

In summary, we have shown that *BIN1* promotes neuronal firing in a Tau-dependent manner. These data contribute new insights into the neuronal functions of *BIN1*, with implications for our understanding of AD.

## Materials and methods

### Key resources table

Reagent type (species) or resource	Designation	Source or reference	Identifiers	Additional information
Gene ( <i>Homo sapiens</i> )	<i>BIN1</i>	NCBI	Gene ID 274	
Antibody	Anti-NeuN Rabbit polyclonal	abcam	Cat# ab104225; RRID:AB_10711153	ICC (1:500), Lot #GR3321966-1
Antibody	Anti-GAD67 Mouse monoclonal	Millipore Sigma	Cat# MAB5406; RRID:AB_2278725	ICC (1:500), Lot #3015328
Antibody	Anti-BIN1 Rabbit polyclonal	Santa Cruz	Cat# sc-30099; RRID:AB_2243399	ICC/PLA/IP (1:500), Lot #K1605; H-100
Antibody	Anti-LVGCC- $\beta$ 1 Mouse monoclonal	abcam	Cat# ab85020; RRID:AB_1861569	ICC/PLA/IP (1:1000), Lot #413-8RR-52
Antibody	Anti-Tau Rabbit polyclonal	DAKO	Cat# A0024; RRID:AB_10013724	ICC/IP (1:1000), Lot #20031827
Antibody	Anti-BIN1 Mouse monoclonal	Santa Cruz	Cat# sc-13575; RRID:AB_626753	ICC/IP (1:1000), Lot #L3014; 99D
Cell line ( <i>Rattus norvegicus</i> )	Primary neuron	Charles River		Fresh from E19 albino Sprague Dawley rats
Genetic reagent	AAV-BIN1-mKate2	UPenn Vector Core		AAV2
Genetic reagent	AAV-mKate2	UPenn Vector Core		AAV2

Continued on next page

Continued

Reagent type (species) or resource	Designation	Source or reference	Identifiers	Additional information
Sequence-based reagent	Tau ASO	PMID: <a href="#">23904623</a> IDT		5-ATCACTGATTTTGAAGTCCC-3
Sequence-based reagent	Scrambled ASO	PMID: <a href="#">23904623</a> IDT		5-CCTTCCCTGAAGTTCTCC-3
Commercial assay, kit	Duolink PLA kit	Millipore Sigma	Cat#s DUO92014; DUO92002; DUO92004	
Transfected construct	GCaMP6f	Addgene	RRID: <a href="#">Addgene_40755</a>	
Transfected construct	mKate2	PMID: <a href="#">25156556</a> Evrogen	Cat# FP184	Actin was removed from the construct obtained
Transfected construct ( <i>Homo sapiens</i> )	BIN1	Horizon Discovery ORFeome Collaboration Clones	OHS5894-202501160	Isoform 1
Cell line ( <i>Cricetulus griseus</i> )	CHO-K1	Millipore Sigma	Cat# 85051005-1VL	Chinese Hamster Ovary cell line
Transfected construct	mKate2-Tau-mKate2	PMID: <a href="#">25156556</a>		
Transfected construct	Fyn-SH3-CBG	PMID: <a href="#">25156556</a>		BIN1-SH3 or LVGCC- $\beta$ 1-SH3 was cloned in replacing Fyn-SH3
Transfected construct ( <i>Homo sapiens</i> )	BIN1-SH3	IDT	AAC28646.1	Codon optimized
Transfected construct ( <i>Homo sapiens</i> )	LVGCC- $\beta$ 1-SH3	IDT	AAA35632.1	Codon optimized

### Primary neuron cultures

Primary hippocampal culture protocols were adapted from [Rush et al., 2020](#). Briefly, hippocampal tissue from E19 Sprague Dawley albino rat (*Rattus norvegicus*) embryos was harvested on ice in 4°C Hibernate E (Life Technologies, A1247601) and digested with 20 units/mL papain (Worthington Biochemical Corporation, LK003178) for 10 min at 37°C. Neurons were then dissociated by manual trituration to a single-cell suspension in Neurobasal medium (Life Technologies, 21103049) supplemented with 1x B-27 (Gibco, 17504044), 2 mM L-Glutamine (Life Technologies, 25030081) and 10% premium select fetal bovine serum (Atlanta Biologicals, S11550). Neuronal plating conditions depended on the experiment, as follows.

### Multi electrode array cultures

For 6-well multielectrode array recordings, neurons were plated at 100,000 per well in six-well MEA plates (ALA Scientific, ALAMEA-MEMMR5). For 48-well plate multielectrode array recordings, neurons were plated at 30,000 per well in 48-well MEA plates (Axion Biosystems, M768-tMEA-48B-5).

### Calcium imaging, electrophysiology, and immunocytochemistry cultures

Neurons were plated at 50,000 neurons per well on 12 mm coverslips (Carolina Biological, 633029) in 24-well plates coated overnight at 4°C with 0.1 mg/mL Poly-D-Lysine (Sigma, P6407–10 × 5 MG) and 0.2 mg/mL laminin (Sigma, L2020-1MG) 24–48 hr prior to the neuron harvest, with the outer wells containing autoclaved ultrapure water (MilliQ filtered) to prevent evaporation.

## Immunoblotting

Neurons were plated at 200,000 per well in six-well plates (Corning, 08-772-1B) and maintained in a 37°C humidified incubator with 5% CO<sub>2</sub>. 24 hr after plating, 75% of the medium was exchanged for serum-free Neurobasal supplemented with B-27 and L-Glutamine, with 5 μM cytosine β-D-arabino-furanoside (AraC, Sigma Aldrich, C6645) to inhibit glial proliferation. 50% medium changes were performed weekly with Neurobasal supplemented with B-27 and L-Glutamine until experiments were started at DIV 19–21.

## BIN1 constructs and vectors

A BIN1-mKate2 (GE Dharmacon, OHS5894-202501160) construct was developed to encode human BIN1 isoform 1 (593 AA, the major neuronal isoform) tagged with mKate2 (Evrogen, FP184, to allow for fluorescent visualization) at the C-terminus to allow for proper function of the N-terminal membrane-interacting BAR domain. A similar construct lacking the BAR domain (amino acids 32–273, BIN1-ΔBAR-mKate2) was produced as a BIN1 BAR domain deletion mutant. A construct encoding mKate2 only was used as a control. These constructs were then cloned into the CIGW vector (rAAV9-CBA-IRES-GFP-WPRE-rBG) (*St Martin et al., 2007*). Due to size limitations for efficient gene expression, the IRES-GFP was removed from the CIGW vector.

## Neuronal transduction

BIN1-mKate2 and mKate2 vectors were packaged into rAAV2 at the University of Pennsylvania Vector Core (stock titers: AAV-BIN1-mKate2: 3.2e12 genomes/ml, AAV-mKate2: 9.69e12 genomes/ml; used titers: AAV-BIN1-mKate2 and AAV-mKate2: 1e10 genomes/ml, used MOI: AAV-BIN1-mKate2 and AAV-mKate2: 200,000). AAV vectors were used in MEA and electrophysiology experiments. Neuronal cultures were transduced on DIV 2.

## Neuronal transfection

BIN1-mKate2, BIN1-ΔBAR-mKate2, and mKate2 vectors were used in transient transfections in calcium imaging experiments. Transfections were performed at DIV 14 using a calcium phosphate precipitation protocol adapted from *Frandemiche et al., 2014*. Briefly, Neurobasal medium was removed and kept until the last step of transfection used as conditioned Neurobasal medium. Neurons were washed for 1–1.5 hr in DMKY buffer containing 1 mM kynurenic acid, 0.9 mM NaOH, 0.5 mM HEPES, 10 MgCl<sub>2</sub>, plus phenol red 0.05%, pH 7.4. Then, 3.5 μg of the vectors were mixed with 120 mM CaCl<sub>2</sub> in HBSS (Life Technologies, 14175095) containing 25 mM HEPES, 140 mM NaCl, and 0.750 mM Na<sub>2</sub>HPO<sub>4</sub>, pH 7.06, left for 20 min to precipitate the DNA, and applied to the primary hippocampal cultures for 30 min. The medium was then replaced with conditioned Neurobasal medium (Life Technologies, 21103049) and cultures were returned to the incubator until use.

## Multielectrode array recordings

### Multi Channel Systems MEA

MEA recording protocols were adapted from *Savell et al., 2019b*. Briefly, E19 rat hippocampal neurons were seeded to six-well MEAs containing nine extracellular recording electrodes and a ground electrode. Neurons were transduced with AAV expressing BIN1 or control constructs on DIV2. Transduced neurons had 50% medium changes with BrainPhys (StemcellTech, 05793) medium supplemented with N2A and SM1 at DIV 5 and 9 to promote maturation, then with supplemented Neurobasal (Life Technologies, 21103049) at DIV 12. 20 min MEA recordings were performed at DIV 12–13 in the temperature-controlled headstage at 37°C. Neuronal firing was amplified and acquired at 30 kHz, digitized, and further analyzed in MC\_Rack (Multi Channel Systems). Data were filtered at 10 Hz and 10,000 Hz filters and thresholded to detect action potentials at each electrode. Detected action potentials were transferred to Offline Sorter (v. 4.0 Plexon) to differentiate multiple neurons detected with a single electrode using principal component analysis (PCA) of waveform properties. Offline Sorter automatically completes and plots PCA on waveforms for each electrode. Manual inspection of PCA, shape, inter-spike intervals, auto-correlograms, and cross-correlograms allowed us to distinguish between multiple units on a single electrode and to do per-neuron analyses. After waveforms were split into units, analysis of each unit's action potential frequency and burst firing was completed in NeuroExplorer (v. 5.0, Plexon) using the built-in Burst Analysis function, with

Poisson burst surprise = 5. Next, firing rates and bursting analysis were performed in NeuroExplorer (v. 5.0 Plexon). Researchers were blinded to experimental conditions performed in all MEA analyses.

### Axion Biosciences MEA

Single neuron electrophysiological activity was recorded using an Axion Maestro recording system as in [Savell et al., 2019a](#). Briefly, neurons were plated on the 48-well MEA (Axion Biosystems, M768-tMEA-48B-5) with 16 extracellular recording electrodes and a ground electrode per well at a density of 30,000 neurons per well in Neurobasal medium (5  $\mu$ L) with 10% FBS (Atlanta Biologicals, S11550) and placed in a 37°C incubator with 5% CO<sub>2</sub>. After allowing neurons to attach to the plate for 2 hr, 300  $\mu$ L serum-free Neurobasal (Life Technologies, 21103049) was added. The next day, AraC was added as with other experiments and a 50% medium change with BrainPhys (Stemcell Technologies Inc, 05790) supplemented with SM1 and L-glutamine was done at DIV 5. At DIV 6, neurons were treated with ASO to reduce Tau protein levels. At DIV 9, a 50% medium change was completed with supplemented BrainPhys, followed by a 50% medium change with supplemented Neurobasal at DIV 12. At DIV 13, neurons were recorded using Axion AxIS software for 15 min. Electrical activity was measured by an interface board at 12.5 kHz, digitized, and transmitted to an external computer for data acquisition and analysis in Axion AxIS Navigator software (Axion Biosystems). All data were filtered using dual 0.01 Hz (high pass) and 5,000 Hz (low-pass) Butterworth filters. Action potential thresholds were set automatically using an adaptive threshold for each electrode (>6 standard deviations from the electrode's mean signal). Neuronal waveforms collected in Axion AxIS Navigator were exported to Offline Sorter (v. 4.0 Plexon). Offline Sorter automatically completes and plots PCA on waveforms for each electrode. Manual inspection of PCA, shape, inter-spike intervals, auto-correlograms, and cross-correlograms allowed us to distinguish between multiple units on a single electrode and to do per-neuron analyses. After waveforms were split into units, analysis of each unit's action potential frequency and burst firing was completed in NeuroExplorer (v. 5.0, Plexon) using the built-in Burst Analysis function, with Poisson burst surprise = 5. Next, firing rates and bursting analysis were performed in NeuroExplorer (v. 5.0 Plexon). Researchers were blinded to experimental conditions performed in all MEA analyses.

### Antisense oligonucleotide application

Tau anti-sense oligonucleotide (ASO) sequences were adapted from [DeVos et al., 2013](#) and produced by Integrated DNA Technology (Tau ASO: 5-ATCACTGATTTTGAAGTCCC-3, Nontargeting control ASO: 5-CCTTCCCTGAAGGTTCTCC-3). ASOs were dissolved to 100  $\mu$ M in 10 mM Tris with 0.1 mM EDTA and stored at -20°C until use. At DIV 6, one week before testing for both MEA experiments and PLA, neurons were treated with ASO to a final concentration of 1  $\mu$ M.

### Calcium imaging

Calcium imaging was adapted from [Léveillé et al., 2008](#). Briefly, rat primary hippocampal neurons (DIV 14) were transfected (see Neuronal transfection section) with the genetically engineered calcium sensor GCaMP6f (gift from Dr. Alain Buisson, originally developed by Douglas Kim and GENIE Project, Addgene plasmid #40755, [Chen et al., 2013](#)). At DIV 21, the neurons were incubated for 15 min at room temperature in HEPES and bicarbonate buffered saline solution (HBBSS) containing 116 mM NaCl, 5.4 mM KCl, 1.8 mM CaCl<sub>2</sub>, 0.8 mM MgSO<sub>4</sub>, 1.3 mM NaH<sub>2</sub>PO<sub>4</sub>, 12 mM HEPES, 5.5 mM glucose, 25 mM bicarbonate and 10  $\mu$ M glycine at pH 7.45. Neurons that were transfected with mKate2 or BIN1-mKate2 vectors (see BIN1 constructs and vectors section) were recorded for 8 min. Experiments were performed at room temperature with continuous perfusion at 2 ml/min with a peristaltic pump, on the stage of a Nikon A1R Confocal (Nikon, TE2000) inverted microscope equipped with a 100 W mercury lamp and oil-immersion Nikon 40x objective with 1.3 numerical aperture (Nikon, Tokyo, Japan). GCaMP6f (excitation: 340/380 nm, emission: 510 nm) ratio images were acquired at 8 Hz with a digital camera (Princeton Instruments, Trenton, NJ) using Metafluor 6.3 software (Universal Imaging Corporation, West Chester, PA, USA). Fluorescence ratios (340/380 nm) were converted to intracellular Ca<sup>2+</sup> concentration using the following formula:

$$[Ca^{2+}]_i = K_d \left( \frac{R - R_{min}}{R_{max} - R} \right) \left( \frac{F_0}{F_s} \right)$$



where  $R$  is the measured ratio of 340/380 fluorescence,  $R_{\min}$  is the ratio measured in a  $\text{Ca}^{2+}$ -free solution,  $R_{\max}$  is the ratio measured in a saturated  $\text{Ca}^{2+}$  solution,  $K_d = 135$  nM (the dissociation constant for GCaMP6f), and  $F_0$  and  $F_s$  are the fluorescence intensities measured at 380 nm, respectively, in a  $\text{Ca}^{2+}$ -free solution or in a saturated  $\text{Ca}^{2+}$  solution.

## Electrophysiology

All electrophysiological recordings were performed in primary hippocampal neuronal cultures after 19–21 DIV. Whole-cell patch-clamp recordings were made from visually identified pyramidal neurons. Recorded signals were amplified with a MultiClamp 700B amplifier (Molecular Devices), filtered at 5 kHz, and sampled at 10 kHz with Digidata 1550A (Molecular Devices). Recordings were acquired using pClamp (v.10) and analyzed using Clampfit (Molecular Devices). Patch pipettes had a resistance of 2.5–5 M $\Omega$  when filled with the internal solution required for the experiments described below. All recordings were performed at room temperature (21–23°C). Internal solution included 120 mM Cs-gluconate, 0.6 mM EGTA, 2.8 mM NaCl, 5 mM MgCl<sub>2</sub>, 2 mM ATP, 0.3 mM GTP, 20 mM HEPES, and 5.0 mM QX-314. External solution included 119 mM NaCl, 2.5 mM KCl, 1.3 mM MgSO<sub>4</sub>, 2.5 mM CaCl<sub>2</sub>, 1 mM NaH<sub>2</sub>PO<sub>4</sub>, 26 mM NaHCO<sub>3</sub>, 11 mM glucose (pH 7.3). Voltage-clamp recordings to measure sEPSCs were performed from cultured neurons by whole-cell patch-clamp holding the neurons at  $-70$  mV with 100  $\mu\text{M}$  picrotoxin (GABA<sub>A</sub>R antagonist, Tocris, 11–281 G) in the bath solution. Voltage-clamp recordings to measure sIPSCs were performed from cultured neurons by whole-cell patch-clamp holding the neurons at 0 mV in 10  $\mu\text{M}$  DNQX (AMPA antagonist, Sigma, D0540-25MG), 100  $\mu\text{M}$  APV (NMDAR antagonist, Tocris, 01-055-0), and 10  $\mu\text{M}$  nifedipine (L-type VGCC antagonist, Sigma, N7634-25G) to enrich for sIPSCs from spontaneously active interneurons rather than from interneuron-driven by excitatory transmission.

## Immunocytochemistry (ICC) and NeuN quantification

ICC was adapted from *Rush et al., 2020*. Briefly, primary neurons on coverslips were fixed with 4% PFA and 4% sucrose in 1x PBS. Coverslips were permeabilized with 0.25% Triton X-100 in 1x PBS for 10 min at room temperature then blocked for one hour in 5% FBS in 1x PBS. Primary antibody for NeuN (abcam, ab104225, 1:500), GAD67 (Millipore Sigma, MAB5406, 1:500), BIN1 (Santa Cruz, sc-30099, 1:500), or LVGCC- $\beta$ 1 (Abcam, S7-18, 1:1,000) in 1% FBS in 1x PBS was applied overnight at 4°C. Coverslips were then washed 3  $\times$  5 min in 1x PBS, then incubated in Alexa Fluor fluorescent antibodies (1:1,000) in 1% FBS in 1x PBS for 1 hr at room temperature. Coverslips were washed 3  $\times$  5 min in 1x PBS, then mounted in Prolong Diamond. For neuron quantification, 10  $\times$  10 images at 20x were taken with an epifluorescent microscope and automatically stitched together using Nikon NIS-Elements. NeuN images were thresholded in ImageJ, then quantified using ImageJ (v. 2.0.0-rc-69/1.52 p) particle analyzer.

## Proximity Ligation Assay (PLA)

PLA was adapted from *Rush et al., 2020*. Briefly, neurons on coverslips were fixed and permeabilized as with ICC, then were incubated overnight with primary antibodies for BIN1 (Santa Cruz, sc-30099, 1:500) and LVGCC- $\beta$ 1 (Abcam, S7-18, 1:1,000) overnight at 4°C, then PLA was performed using the Duolink In Situ Fluorescence kit (Sigma, DUO92004-100RXN). After PLA, coverslips were incubated with secondary antibody to view BIN1 and mounted with Duolink In Situ Mounting Medium with DAPI. Fluorescent images were taken using an epifluorescence microscope at 60x with four channels: DAPI (nuclei), FITC (PLA), and TRITC (mKate2). 7–9 images per slide were obtained and analyzed using ImageJ (v. 2.0.0-rc-69/1.52 p). PLA puncta were quantified using ImageJ particle analyzer, and the average number of puncta per field of view (FOV) or each coverslip was used for analysis.

## Bioluminescence Resonance Energy Transfer (BRET)

BRET was conducted as described in *Cochran et al., 2014*. Codon-optimized human BIN1-SH3 or LVGCC- $\beta$ 1-SH3 domains were fused on the C-terminus to click beetle green (CBG) luciferase (Promega, E1461) replacing the Fyn-SH3 in the previously described donor construct. Tau tagged at each terminus with mKate2 (Evrogen, FP184) served as the acceptor. Chinese hamster ovary (CHO) cells (Sigma, 85051005-1VL) obtained from ECACC (Lot number 12G006) were authenticated using DNA

Fingerprinting and DNA bar-coding sequencing and tested negative for mycoplasma contamination using PCR, a Vero indicator cell line, and Hoechst 33258 fluorescent detection system (Certificate of Analysis test number 47856). CHO cells were plated in 24-well opaque white plates (Promega, 6005168) using the manufacturer's instructions and transfected with donor and acceptor constructs using Fugene. Forty-eight hours later, fluorescence was read by excitation with a 530/25 nm filter and emission with a 645/40 nm filter on a Synergy2 (BioTek) to control for the concentration of the donor. Immediately after fluorescence measurement, D-luciferin (Promega, E1605) was added to a final concentration of 200  $\mu$ M to each well. Two to 4 hr later, after the signal had stabilized, plates were read with 645/40 nm filter. Measured BRET fluorescence was normalized to mKate2 fluorescence.

## Co-immunoprecipitation

Mouse hemibrains were finely chopped while frozen, then thawed on ice in PBS plus protease inhibitors (Fisher PI-78439), phosphatase inhibitors (Sigma-Aldrich, P5726), and 1 mM of the cell-permeable cross-linker DSP (Fisher, PI-22585). Hemibrains were then homogenized for 15 s using a hand-held Kontes Pellet Pestle homogenizer, then pipetted up and down 20x to obtain a smooth lysate. Lysates were spun 2  $\times$  10 min at 800  $\times$  g, then cleared lysates were incubated for 15 min at 4°C on an end-over-end rotator. Next, lysates were brought to 100 mM Tris to inactivate DSP and incubated for another 15 min at 4°C on an end-over-end rotator. Samples were then diluted 1:1 with a mild co-IP buffer: 10 mM Tris (pH 7.5), 10 mM NaCl, 3 mM MgCl<sub>2</sub>, 1 mM EGTA, and 0.05% Nonidet P-40, a mild lysis buffer previously shown to be amenable to co-IP experiment (Filiano *et al.*, 2008). At this point, an input fraction was set aside before adding IP antibody to the lysate, with 5  $\mu$ g of antibody used in each case. Lysate/antibody mixtures were incubated overnight on an end-over-end rotator. Next, 50  $\mu$ L of Protein G-coated magnetic beads (Life Technologies, 10004D) were added and incubated for 8 hr at 4°C on an end-over-end rotator. Next, non-interacting lysate was removed, the bead/antibody/antigen complex was washed, then protein was eluted with 50 mM Glycine (pH 2.8) and neutralized with 1 M Tris, reduced with  $\beta$ -Mercaptoethanol and an 80°C incubation for 10 min, then cooled and probed by immunoblotting.

## Immunoblots

5  $\mu$ g of immunoprecipitated samples were loaded and separated on 4–12% NuPage acrylamide gels (Invitrogen) with NuPage MOPS running buffer for 2 hr at 110 V. Next, proteins were transferred to Immobilon-FL PVDF membranes (Millipore) using the NuPage transfer buffer transfer system (Invitrogen) overnight. The membrane was blocked in LI-COR Odyssey blocking buffer (LI-COR, 927–40000) for 1 hr at room temperature and incubated with the appropriate primary antibody. After primary antibody treatment, membranes were washed three times in tris-buffered saline with 0.1% Tween (TBS-T), followed by incubation for 1 hr with Alexa Fluor 700- or 800-conjugated goat antibodies specific for mouse immunoglobulin G (1:20,000, LI-COR). Membranes were then washed three times in TBS-T, followed by a single wash in TBS, imaged on the LI-COR Odyssey fluorescence imaging system, and quantified using LI-COR Image Studio (v. 5.2.5).

## Animals

All breeding and experimental procedures were approved by the University of Alabama at Birmingham Institutional Animal Care and Use Committee and follow the guidelines by the National Institutes of Health. Male and female Tau<sup>+/-</sup> mice lacking exon 1 of MAPT gene were bred to obtain Tau<sup>-/-</sup> mice with littermate Tau<sup>+/+</sup> controls. Mice were maintained under standard laboratory conditions (12 hr light/dark cycle, 50% humidity, Harlan 2916 diet, and water ad libitum). Genotype was verified by standard PCR protocol.

## Statistics

Statistical distribution of data varied widely between data sets in this study, so we analyzed each data set for normality and analyzed using either parametric or non-parametric tests accordingly. The specific test used is indicated in the figure legend in each case. All statistical tests were performed with Prism 8 (GraphPad, v. 8.4.0).

## Acknowledgements

We thank all members of the Roberson lab for helpful discussions and critiques, and Andy West, David Standaert, and Alain Buisson for plasmids. This work was supported by the National Institutes of Health grants RF1AG059405, R01NS075487, R01MH114990, T32NS095775, and T32NS061788, the Alzheimer's Association, and the Weston Brain Institute. The authors declare no financial interests. EDR is an owner of intellectual property relating to Tau.

## Additional information

### Competing interests

Erik D Roberson: EDR is an owner of intellectual property relating to Tau. The other authors declare that no competing interests exist.

### Funding

Funder	Grant reference number	Author
National Institutes of Health	RF1AG059405	Erik D Roberson
National Institutes of Health	R01NS075487	Erik D Roberson
National Institutes of Health	R01MH114990	Jeremy J Day
National Institutes of Health	T32NS095775	Yuliya Voskobiynk
National Institutes of Health	T32NS061788	Jonathan R Roth
Alzheimer's Association		Erik D Roberson
Weston Brain Institute		Jonathan R Roth Travis Rush Erik D Roberson

The funders had no role in study design, data collection and interpretation, or the decision to submit the work for publication.

### Author contributions

Yuliya Voskobiynk, Conceptualization, Resources, Data curation, Software, Formal analysis, Supervision, Funding acquisition, Validation, Investigation, Visualization, Methodology, Writing - original draft, Project administration, Writing - review and editing; Jonathan R Roth, Data curation, Software, Funding acquisition, Validation, Investigation, Visualization, Methodology, Project administration, Writing - review and editing; J Nicholas Cochran, Travis Rush, Data curation, Software, Formal analysis, Validation, Visualization, Methodology, Writing - review and editing; Nancy VN Carullo, Data curation, Software, Formal analysis, Supervision, Methodology, Writing - review and editing; Jacob S Mesina, Mohammad Waqas, Rachael M Vollmer, Data curation, Formal analysis, Writing - review and editing; Jeremy J Day, Resources, Software, Supervision, Funding acquisition, Writing - review and editing; Lori L McMahon, Methodology, Writing - review and editing; Erik D Roberson, Conceptualization, Resources, Formal analysis, Supervision, Funding acquisition, Investigation, Methodology, Project administration, Writing - review and editing

### Author ORCIDs

Yuliya Voskobiynk  <https://orcid.org/0000-0003-4169-3002>  
 Jonathan R Roth  <https://orcid.org/0000-0001-8978-4507>  
 Nancy VN Carullo  <http://orcid.org/0000-0001-9197-5046>  
 Jeremy J Day  <http://orcid.org/0000-0002-7361-3399>  
 Lori L McMahon  <http://orcid.org/0000-0003-1104-6584>  
 Erik D Roberson  <https://orcid.org/0000-0002-1810-9763>

### Ethics

Animal experimentation: This study was performed in strict accordance with the recommendations in the Guide for the Care and Use of Laboratory Animals of the National Institutes of Health. All of the animals were handled according to approved institutional animal care and use committee (IACUC) protocols (#20450) of the University of Alabama at Birmingham. The protocol was approved by the Committee on the Ethics of Animal Experiments of the University of Alabama at Birmingham.

### Decision letter and Author response

Decision letter <https://doi.org/10.7554/eLife.57354.sa1>

Author response <https://doi.org/10.7554/eLife.57354.sa2>

## Additional files

### Supplementary files

- Transparent reporting form

### Data availability

All data generated or analysed during this study are included in the manuscript and supporting files. Source data files have been provided for Figures 6; high throughput raw electrophysiologic recordings of neuronal activity using Axion Biosciences Maestro are deposited on Dryad at <https://doi.org/10.5061/dryad.rbnzs7h8z>. Brief Analysis used is described in the methods section; in-depth analysis description is publicly available at <https://www.axionbiosystems.com/products/software/neural-module>.

The following dataset was generated:

Author(s)	Year	Dataset title	Dataset URL	Database and Identifier
Voskobiyuk Y, Roth JR, Cochran JN, Rush T, Carullo NVN, Mesina JS, Waqas M, Vollmer RM, Day JJ, McMahan LL, Robertson ED	2020	Data from: Alzheimer's disease risk gene <i>BIN1</i> induces Tau-dependent network hyperexcitability	<a href="https://doi.org/10.5061/dryad.rbnzs7h8z">https://doi.org/10.5061/dryad.rbnzs7h8z</a>	Dryad Digital Repository, 10.5061/dryad.rbnzs7h8z

## References

- Amatniek JC**, Hauser WA, DelCastillo-Castaneda C, Jacobs DM, Marder K, Bell K, Albert M, Brandt J, Stern Y. 2006. Incidence and predictors of seizures in patients with Alzheimer's disease. *Epilepsia* **47**:867–872. DOI: <https://doi.org/10.1111/j.1528-1167.2006.00554.x>, PMID: 16686651
- Beecham GW**, Hamilton K, Naj AC, Martin ER, Huentelman M, Myers AJ, Corneveaux JJ, Hardy J, Vonsattel J-P, Younkin SG, Bennett DA, De Jager PL, Larson EB, Crane PK, Kambh MI, Kofler JK, Mash DC, Duque L, Gilbert JR, Gwirtsman H, et al. 2014. Genome-Wide Association Meta-analysis of Neuropathologic Features of Alzheimer's Disease and Related Dementias. *PLOS Genetics* **10**:e1004606. DOI: <https://doi.org/10.1371/journal.pgen.1004606>
- Benson DL**, Watkins FH, Steward O, Banker G. 1994. Characterization of GABAergic neurons in hippocampal cell cultures. *Journal of Neurocytology* **23**:279–295. DOI: <https://doi.org/10.1007/BF01188497>, PMID: 8089704
- Bookheimer SY**, Strojwas MH, Cohen MS, Saunders AM, Pericak-Vance MA, Mazziotta JC, Small GW. 2000. Patterns of brain activation in people at risk for Alzheimer's disease. *New England Journal of Medicine* **343**: 450–456. DOI: <https://doi.org/10.1056/NEJM200008173430701>, PMID: 10944562
- Bretteville A**, Demiautte F, Chapuis J. 2017. Proximity ligation assay: a tool to study endogenous interactions between tau and its neuronal partners. *Methods in Molecular Biology* **1523**:297–305. DOI: [https://doi.org/10.1007/978-1-4939-6598-4\\_18](https://doi.org/10.1007/978-1-4939-6598-4_18), PMID: 27975258
- Brown JT**, Chin J, Leiser SC, Pangalos MN, Randall AD. 2011. Altered intrinsic neuronal excitability and reduced  $Na^+$  currents in a mouse model of Alzheimer's disease. *Neurobiology of Aging* **32**:2109.e1–212109. DOI: <https://doi.org/10.1016/j.neurobiolaging.2011.05.025>
- Bungenberg J**, Surano N, Grote A, Surges R, Pernhorst K, Hofmann A, Schoch S, Helmstaedter C, Becker AJ. 2016. Gene expression variance in hippocampal tissue of temporal lobe epilepsy patients corresponds to

- differential memory performance. *Neurobiology of Disease* **86**:121–130. DOI: <https://doi.org/10.1016/j.nbd.2015.11.011>, PMID: 26631617
- Buraei Z, Yang J. 2010. The  $\beta$  subunit of voltage-gated Ca<sup>2+</sup> channels. *Physiological Reviews* **90**:1461–1506. DOI: <https://doi.org/10.1152/physrev.00057.2009>, PMID: 20959621
- Butler MH, David C, Ochoa GC, Freyberg Z, Daniell L, Grabs D, Cremona O, De Camilli P. 1997. Amphiphysin II (SH3P9; BIN1), a member of the amphiphysin/Rvs family, is concentrated in the cortical cytomatrix of axon initial segments and nodes of ranvier in brain and around T tubules in skeletal muscle. *Journal of Cell Biology* **137**:1355–1367. DOI: <https://doi.org/10.1083/jcb.137.6.1355>, PMID: 9182667
- Carrasquillo MM, Belbin O, Hunter TA, Ma L, Bisceglia GD, Zou F, Crook JE, Pankratz VS, Sando SB, Aasly JO, Barcikowska M, Wszolek ZK, Dickson DW, Graff-Radford NR, Petersen RC, Morgan K, Younkin SG. 2011. Replication of BIN1 association with Alzheimer's disease and evaluation of genetic interactions. *Journal of Alzheimer's Disease* **24**:751–758. DOI: <https://doi.org/10.3233/JAD-2011-101932>, PMID: 21321396
- Cataldi M. 2013. The changing landscape of voltage-gated calcium channels in neurovascular disorders and in neurodegenerative diseases. *Current Neuropharmacology* **11**:276–297. DOI: <https://doi.org/10.2174/1570159X11311030004>, PMID: 24179464
- Chapuis J, Hansmannel F, Gistelinc M, Mounier A, Van Cauwenberghe C, Kolen KV, Geller F, Sottejeau Y, Harold D, Dourlen P, Grenier-Boley B, Kamatani Y, Delepine B, Demiautte F, Zelenika D, Zommer N, Hamdane M, Bellenguez C, Dartigues JF, Hauw JJ, et al. 2013. Increased expression of BIN1 mediates alzheimer genetic risk by modulating tau pathology. *Molecular Psychiatry* **18**:1225–1234. DOI: <https://doi.org/10.1038/mp.2013.1>, PMID: 23399914
- Chen TW, Wardill TJ, Sun Y, Pulver SR, Renninger SL, Baohan A, Schreiter ER, Kerr RA, Orger MB, Jayaraman V, Looger LL, Svoboda K, Kim DS. 2013. Ultrasensitive fluorescent proteins for imaging neuronal activity. *Nature* **499**:295–300. DOI: <https://doi.org/10.1038/nature12354>, PMID: 23868258
- Chibnik LB, Yu L, Eaton ML, Srivastava G, Schneider JA, Kellis M, Bennett DA, De Jager PL. 2015. Alzheimer's loci: epigenetic associations and interaction with genetic factors. *Annals of Clinical and Translational Neurology* **2**:636–647. DOI: <https://doi.org/10.1002/acn3.201>, PMID: 26125039
- Chin J, Roberson ED, Mucke L. 2007. Molecular aspects of memory dysfunction in Alzheimer's disease. In: Byrne J (Ed). *Learning and Memory: A Comprehensive Reference*. Academic Press. p. 245–293. DOI: <https://doi.org/10.1016/B978-012370509-9.00015-2>
- Cochran JN, Diggs PV, Nebane NM, Rasmussen L, White EL, Bostwick R, Maddry JA, Suto MJ, Roberson ED. 2014. AlphaScreen HTS and live-cell bioluminescence resonance energy transfer (BRET) assays for identification of Tau-Fyn SH3 interaction inhibitors for alzheimer disease. *Journal of Biomolecular Screening* **19**:1338–1349. DOI: <https://doi.org/10.1177/1087057114547232>, PMID: 25156556
- De Jager PL, Srivastava G, Lunnon K, Burgess J, Schalkwyk LC, Yu L, Eaton ML, Keenan BT, Ernst J, McCabe C, Tang A, Raj T, Replogle J, Brodeur W, Gabriel S, Chai HS, Younkin C, Younkin SG, Zou F, Szyf M, et al. 2014. Alzheimer's disease: early alterations in brain DNA methylation at ANK1, BIN1, RHBDF2 and other loci. *Nature Neuroscience* **17**:1156–1163. DOI: <https://doi.org/10.1038/nn.3786>, PMID: 25129075
- De Rossi P, Buggia-Prévoit V, Clayton BL, Vasquez JB, van Sanford C, Andrew RJ, Lesnick R, Botté A, Deyts C, Salem S, Rao E, Rice RC, Parent A, Kar S, Popko B, Pytel P, Estus S, Thinakaran G. 2016. Predominant expression of Alzheimer's disease-associated BIN1 in mature oligodendrocytes and localization to white matter tracts. *Molecular Neurodegeneration* **11**:59. DOI: <https://doi.org/10.1186/s13024-016-0124-1>, PMID: 27488240
- De Rossi P, Nomura T, Andrew RJ, Masse NY, Sampathkumar V, Musial TF, Sudwars A, Recupero AJ, Le Metayer T, Hansen MT, Shim HN, Krause SV, Freedman DJ, Bindokas VP, Kasthuri N, Nicholson DA, Contractor A, Thinakaran G. 2020. Neuronal BIN1 regulates presynaptic neurotransmitter release and memory consolidation. *Cell Reports* **30**:3520–3535. DOI: <https://doi.org/10.1016/j.celrep.2020.02.026>, PMID: 32160554
- DeVos SL, Goncharoff DK, Chen G, Kebodeaux CS, Yamada K, Stewart FR, Schuler DR, Maloney SE, Wozniak DF, Rigo F, Bennett CF, Cirrito JR, Holtzman DM, Miller TM. 2013. Antisense reduction of tau in adult mice protects against seizures. *Journal of Neuroscience* **33**:12887–12897. DOI: <https://doi.org/10.1523/JNEUROSCI.2107-13.2013>, PMID: 23904623
- Dickerson BC, Salat DH, Greve DN, Chua EF, Rand-Giovannetti E, Rentz DM, Bertram L, Mullin K, Tanzi RE, Blacker D, Albert MS, Sperling RA. 2005. Increased hippocampal activation in mild cognitive impairment compared to normal aging and AD. *Neurology* **65**:404–411. DOI: <https://doi.org/10.1212/01.wnl.0000171450.97464.49>, PMID: 16087905
- Dong X, Zhang L, Meng Q, Gao Q. 2016. Association between Interleukin-1A, Interleukin-1B, and bridging integrator 1 polymorphisms and Alzheimer's disease: A standard and cumulative meta-analysis. In: *Mol Neurobiol* **54**:736–747. DOI: <https://doi.org/10.1007/s12035-015-9683-3>
- Filiano AJ, Bailey CD, Tucholski J, Gundemir S, Johnson GV. 2008. Transglutaminase 2 protects against ischemic insult, interacts with HIF1beta, and attenuates HIF1 signaling. *The FASEB Journal* **22**:2662–2675. DOI: <https://doi.org/10.1096/fj.07-097709>, PMID: 18375543
- Frandemiche ML, De Seranno S, Rush T, Borel E, Elie A, Arnal I, Lanté F, Buisson A. 2014. Activity-dependent tau protein translocation to excitatory synapse is disrupted by exposure to amyloid-beta oligomers. *Journal of Neuroscience* **34**:6084–6097. DOI: <https://doi.org/10.1523/JNEUROSCI.4261-13.2014>, PMID: 24760868
- Franzmeier N, Rubinski A, Neitzel J, Ewers M, Alzheimer's Disease Neuroimaging Initiative (ADNI). 2019. The BIN1 rs744373 SNP is associated with increased tau-PET levels and impaired memory. *Nature Communications* **10**:1766. DOI: <https://doi.org/10.1038/s41467-019-09564-5>, PMID: 30992433

- Gheyara AL**, Ponnusamy R, Djukic B, Craft RJ, Ho K, Guo W, Finucane MM, Sanchez PE, Mucke L. 2014. Tau reduction prevents disease in a mouse model of dravet syndrome. *Annals of Neurology* **76**:443–456. DOI: <https://doi.org/10.1002/ana.24230>, PMID: 25042160
- Glennon EBC**, Whitehouse IJ, Miners JS, Kehoe PG, Love S, Kellett KAB, Hooper NM. 2013. BIN1 is decreased in sporadic but not familial Alzheimer's Disease or in Aging. *PLOS ONE* **8**:e78806. DOI: <https://doi.org/10.1371/journal.pone.0078806>
- Hämäläinen A**, Pihlajamäki M, Tanila H, Hänninen T, Niskanen E, Tervo S, Karjalainen PA, Vanninen RL, Soininen H. 2007. Increased fMRI responses during encoding in mild cognitive impairment. *Neurobiology of Aging* **28**: 1889–1903. DOI: <https://doi.org/10.1016/j.neurobiolaging.2006.08.008>, PMID: 16997428
- Harold D**, Abraham R, Hollingworth P, Sims R, Gerrish A, Hamshere ML, Pahwa JS, Moskvina V, Dowzell K, Williams A, Jones N, Thomas C, Stretton A, Morgan AR, Lovestone S, Powell J, Proitsis P, Lupton MK, Brayne C, Rubinsztein DC, et al. 2009. Genome-wide association study identifies variants at CLU and PICALM associated with Alzheimer's disease. *Nature Genetics* **41**:1088–1093. DOI: <https://doi.org/10.1038/ng.440>, PMID: 19734902
- Holler CJ**, Davis PR, Beckett TL, Platt TL, Webb RL, Head E, Murphy MP. 2014. Bridging integrator 1 (BIN1) protein expression increases in the Alzheimer's disease brain and correlates with neurofibrillary tangle pathology. *Journal of Alzheimer's Disease* **42**:1221–1227. DOI: <https://doi.org/10.3233/JAD-132450>, PMID: 25024306
- Hollingworth P**, Harold D, Sims R, Gerrish A, Lambert JC, Carrasquillo MM, Abraham R, Hamshere ML, Pahwa JS, Moskvina V, Dowzell K, Jones N, Stretton A, Thomas C, Richards A, Ivanov D, Widdowson C, Chapman J, Lovestone S, Powell J, et al. 2011. Common variants at ABCA7, MS4A6A/MS4A4E, EPHA1, CD33 and CD2AP are associated with Alzheimer's disease. *Nature Genetics* **43**:429–435. DOI: <https://doi.org/10.1038/ng.803>, PMID: 21460840
- Holth J**, Reed JG, Inoue T, Pautler R, Botas J, Noebels J. 2011. Tau loss regulates excitability in mouse and *Drosophila* genetic models of epilepsy. Society for Neuroscience Abstracts:671.08.
- Hong TT**, Smyth JW, Gao D, Chu KY, Vogan JM, Fong TS, Jensen BC, Colecraft HM, Shaw RM. 2010. BIN1 localizes the L-type calcium channel to cardiac T-tubules. *PLOS Biology* **8**:e1000312. DOI: <https://doi.org/10.1371/journal.pbio.1000312>, PMID: 20169111
- Hong T**, Yang H, Zhang SS, Cho HC, Kalashnikova M, Sun B, Zhang H, Bhargava A, Grabe M, Olgin J, Gorelik J, Marbán E, Jan LY, Shaw RM. 2014. Cardiac BIN1 folds T-tubule membrane, controlling ion flux and limiting arrhythmia. *Nature Medicine* **20**:624–632. DOI: <https://doi.org/10.1038/nm.3543>, PMID: 24836577
- Hu X**, Pickering E, Liu YC, Hall S, Fournier H, Katz E, Dechairo B, John S, Van Eerdewegh P, Soares H, Alzheimer's Disease Neuroimaging Initiative. 2011. Meta-analysis for genome-wide association study identifies multiple variants at the BIN1 locus associated with late-onset Alzheimer's disease. *PLOS ONE* **6**:e16616. DOI: <https://doi.org/10.1371/journal.pone.0016616>, PMID: 21390209
- Ittner LM**, Ke YD, Delerue F, Bi M, Gladbach A, van Eersel J, Wöfling H, Chieng BC, Christie MJ, Napier IA, Eckert A, Staufenbiel M, Hardeman E, Götz J. 2010. Dendritic function of tau mediates amyloid-beta toxicity in Alzheimer's disease mouse models. *Cell* **142**:387–397. DOI: <https://doi.org/10.1016/j.cell.2010.06.036>, PMID: 20655099
- Joutsa J**, Rinne JO, Hermann B, Karrasch M, Anttinen A, Shinnar S, Sillanpää M. 2017. Association between Childhood-Onset epilepsy and amyloid burden 5 decades later. *JAMA Neurology* **74**:583–590. DOI: <https://doi.org/10.1001/jamaneurol.2016.6091>
- Kamboh MI**, Demirci FY, Wang X, Minster RL, Carrasquillo MM, Pankratz VS, Younkin SG, Saykin AJ, Jun G, Baldwin C, Logue MW, Buross J, Farrer L, Pericak-Vance MA, Haines JL, Sweet RA, Ganguli M, Feingold E, Dekosky ST, Lopez OL, et al. 2012. Genome-wide association study of Alzheimer's disease. *Translational Psychiatry* **2**:e117. DOI: <https://doi.org/10.1038/tp.2012.45>, PMID: 22832961
- Keret O**, Hoang TD, Xia F, Rosen HJ, Yaffe K. 2020. Association of Late-Onset unprovoked seizures of unknown etiology with the risk of developing dementia in older veterans. *JAMA Neurology* **77**:710. DOI: <https://doi.org/10.1001/jamaneurol.2020.0187>
- Kuijlaars J**, Oyelami T, Diels A, Rohrbacher J, Versweyveld S, Meneghello G, Tuefferd M, Verstraelen P, Detrez JR, Verschuuren M, De Vos WH, Meert T, Peeters PJ, Cik M, Nuydens R, Brône B, Verheyen A. 2016. Sustained synchronized neuronal network activity in a human astrocyte co-culture system. *Scientific Reports* **6**:36529. DOI: <https://doi.org/10.1038/srep36529>, PMID: 27819315
- Kunkle BW**, Grenier-Boley B, Sims R, Bis JC, Damotte V, Naj AC, Boland A, Vronskaya M, van der Lee SJ, Amlie-Wolf A, Bellenguez C, Frizatti A, Chouraki V, Martin ER, Sleegers K, Badarinarayan N, Jakobsdottir J, Hamilton-Nelson KL, Moreno-Grau S, O'Laso R, et al. 2019. Genetic meta-analysis of diagnosed Alzheimer's disease identifies new risk loci and implicates Aβ, tau, immunity and lipid processing. *Nature Genetics* **51**:414–430. DOI: <https://doi.org/10.1038/s41588-019-0358-2>, PMID: 30820047
- Lambert J-C**, Zelenika D, Hiltunen M, Chouraki V, Combarros O, Bullido MJ, Tognoni G, Fiévet N, Boland A, Arosio B, Coto E, Zompo MD, Mateo I, Frank-Garcia A, Helisalmi S, Porcellini E, Pilotto A, Forti P, Ferri R, Delepine M, et al. 2011. Evidence of the association of BIN1 and PICALM with the AD risk in contrasting European populations. *Neurobiology of Aging* **32**:e11–e15. DOI: <https://doi.org/10.1016/j.neurobiolaging.2010.11.022>
- Lambert JC**, Ibrahim-Verbaas CA, Harold D, Naj AC, Sims R, Bellenguez C, DeStafano AL, Bis JC, Beecham GW, Grenier-Boley B, Russo G, Thornton-Wells TA, Jones N, Smith AV, Chouraki V, Thomas C, Ikram MA, Zelenika D, Vardarajan BN, Kamatani Y, et al. 2013. Meta-analysis of 74,046 individuals identifies 11 new susceptibility loci

- for alzheimer's disease. *Nature Genetics* **45**:1452–1458. DOI: <https://doi.org/10.1038/ng.2802>, PMID: 24162737
- Lasorsa A**, Malki I, Cantrelle FX, Merzougui H, Boll E, Lambert JC, Landrieu I. 2018. Structural basis of tau interaction with BIN1 and regulation by tau phosphorylation. *Frontiers in Molecular Neuroscience* **11**:421. DOI: <https://doi.org/10.3389/fnmol.2018.00421>, PMID: 30487734
- Lee JH**, Cheng R, Barral S, Reitz C, Medrano M, Lantigua R, Jiménez-Velázquez IZ, Rogaeva E, St George-Hyslop PH, Mayeux R. 2011. Identification of novel loci for alzheimer disease and replication of *CLU*, *PICALM*, and *BIN1* in caribbean hispanic individuals. *Archives of Neurology* **68**:320–328. DOI: <https://doi.org/10.1001/archneurol.2010.292>, PMID: 21059989
- Lerdkrai C**, Asavapanumas N, Brawek B, Kovalchuk Y, Mojtabedi N, Olmedillas Del Moral M, Garaschuk O. 2018. Intracellular Ca<sup>2+</sup> stores control in vivo neuronal hyperactivity in a mouse model of alzheimer's disease. *PNAS* **115**:E1279–E1288. DOI: <https://doi.org/10.1073/pnas.1714409115>, PMID: 29358403
- Léveillé F**, El Gaamouch F, Goux E, Lecocq M, Lobner D, Nicole O, Buisson A. 2008. Neuronal viability is controlled by a functional relation between synaptic and extrasynaptic NMDA receptors. *The FASEB Journal* **22**:4258–4271. DOI: <https://doi.org/10.1096/fj.08-107268>, PMID: 18711223
- Li HL**, Yang P, Liu ZJ, Sun YM, Lu SJ, Tao QQ, Guo QH, Wu ZY. 2015. Common variants at Bin1 are associated with sporadic alzheimer's disease in the Han Chinese population. *Psychiatric Genetics* **25**:21–25. DOI: <https://doi.org/10.1097/YPG.0000000000000071>, PMID: 25461955
- Liu G**, Zhang S, Cai Z, Li Y, Cui L, Ma G, Jiang Y, Zhang L, Feng R, Liao M, Chen Z, Zhao B, Li K. 2013. *BIN1* gene rs744373 polymorphism contributes to Alzheimer's disease in East Asian population. *Neuroscience Letters* **544**:47–51. DOI: <https://doi.org/10.1016/j.neulet.2013.02.075>, PMID: 23570733
- Liu Y**, Harding M, Pittman A, Dore J, Striessnig J, Rajadhyaksha A, Chen X. 2014. Cav1.2 and Cav1.3 L-type calcium channels regulate dopaminergic firing activity in the mouse ventral tegmental area. *Journal of Neurophysiology* **112**:1119–1130. DOI: <https://doi.org/10.1152/jn.00757.2013>, PMID: 24848473
- Liu S**, Shen Y, Shultz SR, Nguyen A, Hovens C, Adlard PA, Bush AI, Chan J, Kwan P, O'Brien TJ, Jones NC. 2017. Accelerated kindling epileptogenesis in Tg4510 tau transgenic mice, but not in tau knockout mice. *Epilepsia* **58**:e136–e141. DOI: <https://doi.org/10.1111/epi.13847>, PMID: 28710841
- Logue MW**. 2011. A comprehensive genetic association study of alzheimer disease in african americans. *Archives of Neurology* **68**:1569–1579. DOI: <https://doi.org/10.1001/archneurol.2011.646>
- Malki I**, Cantrelle FX, Sottejeau Y, Lippens G, Lambert JC, Landrieu I. 2017. Regulation of the interaction between the neuronal BIN1 isoform 1 and tau proteins - role of the SH3 domain. *The FEBS Journal* **284**:3218–3229. DOI: <https://doi.org/10.1111/febs.14185>, PMID: 28755476
- McAvoy KM**, Rajamohamed Sait H, Marsh G, Peterson M, Reynolds TL, Gagnon J, Geisler S, Leach P, Roberts C, Cahir-McFarland E, Ransohoff RM, Crotti A. 2019. Cell-autonomous and non-cell autonomous effects of neuronal BIN1 loss in vivo. *PLOS ONE* **14**:e0220125. DOI: <https://doi.org/10.1371/journal.pone.0220125>, PMID: 31408457
- Minkeviciene R**, Rheims S, Dobszay MB, Zilberter M, Hartikainen J, Fulop L, Penke B, Zilberter Y, Harkany T, Pitkanen A, Tanila H. 2009. Amyloid -Induced Neuronal Hyperexcitability Triggers Progressive Epilepsy. *Journal of Neuroscience* **29**:3453–3462. DOI: <https://doi.org/10.1523/JNEUROSCI.5215-08.2009>
- Miyashita A**, Koike A, Jun G, Wang LS, Takahashi S, Matsubara E, Kawarabayashi T, Shoji M, Tomita N, Arai H, Asada T, Harigaya Y, Ikeda M, Amari M, Hanyu H, Higuchi S, Ikeuchi T, Nishizawa M, Suga M, Kawase Y, et al. 2013. *SORL1* is genetically associated with late-onset Alzheimer's disease in Japanese, Koreans and Caucasians. *PLOS ONE* **8**:e58618. DOI: <https://doi.org/10.1371/journal.pone.0058618>, PMID: 23565137
- Morton RA**, Norlin MS, Vollmer CC, Valenzuela CF. 2013. Characterization of L-type voltage-gated ca(2+) channel expression and function in developing CA3 pyramidal neurons. *Neuroscience* **238**:59–70. DOI: <https://doi.org/10.1016/j.neuroscience.2013.02.008>, PMID: 23415785
- Muller AJ**, Baker JF, DuHadaway JB, Ge K, Farmer G, Donover PS, Meade R, Reid C, Grzanna R, Roach AH, Shah N, Soler AP, Prendergast GC. 2003. Targeted disruption of the murine *Bin1/Amphiphysin II* gene does not disable endocytosis but results in embryonic cardiomyopathy with aberrant myofibril formation. *Molecular and Cellular Biology* **23**:4295–4306. DOI: <https://doi.org/10.1128/MCB.23.12.4295-4306.2003>, PMID: 12773571
- Naj AC**, Jun G, Beecham GW, Wang LS, Vardarajan BN, Buross J, Gallins PJ, Buxbaum JD, Jarvik GP, Crane PK, Larson EB, Bird TD, Boeve BF, Graff-Radford NR, De Jager PL, Evans D, Schneider JA, Carrasquillo MM, Ertekin-Taner N, Younkin SG, et al. 2011. Common variants at *MS4A4/MS4A6E*, *CD2AP*, *CD33* and *EPHA1* are associated with late-onset Alzheimer's disease. *Nature Genetics* **43**:436–441. DOI: <https://doi.org/10.1038/ng.801>, PMID: 21460841
- Naj AC**, Jun G, Reitz C, Kunkle BW, Perry W, Park YS, Beecham GW, Rajbhandary RA, Hamilton-Nelson KL, Wang LS, Kauwe JS, Huentelman MJ, Myers AJ, Bird TD, Boeve BF, Baldwin CT, Jarvik GP, Crane PK, Rogaeva E, Barmada MM, et al. 2014. Effects of multiple genetic loci on age at onset in late-onset alzheimer disease: a genome-wide association study. *JAMA Neurology* **71**:1394–1404. DOI: <https://doi.org/10.1001/jamaneurol.2014.1491>, PMID: 25199842
- Nott A**, Holtman IR, Coufal NG, Schlachetzki JCM, Yu M, Hu R, Han CZ, Pena M, Xiao J, Wu Y, Keulen Z, Pasillas MP, O'Connor C, Nickl CK, Schafer ST, Shen Z, Rissman RA, Brewer JB, Gosselin D, Gonda DD, et al. 2019. Brain cell type-specific enhancer-promoter interactome maps and disease-risk association. *Science* **366**:1134–1139. DOI: <https://doi.org/10.1126/science.aay0793>, PMID: 31727856
- Palop JJ**, Chin J, Roberson ED, Wang J, Thwin MT, Bien-Ly N, Yoo J, Ho KO, Yu GQ, Kreitzer A, Finkbeiner S, Noebels JL, Mucke L. 2007. Aberrant excitatory neuronal activity and compensatory remodeling of inhibitory

- hippocampal circuits in mouse models of Alzheimer's disease. *Neuron* **55**:697–711. DOI: <https://doi.org/10.1016/j.neuron.2007.07.025>, PMID: 17785178
- Palop JJ**, Mucke L. 2009. Epilepsy and cognitive impairments in alzheimer disease. *Archives of Neurology* **66**: 435–440. DOI: <https://doi.org/10.1001/archneurol.2009.15>, PMID: 19204149
- Picas L**, Viaud J, Schauer K, Vanni S, Hnia K, Fraiser V, Roux A, Bassereau P, Gaits-lacovoni F, Payrastré B, Laporte J, Manneville JB, Goud B. 2014. BIN1/M-Amphiphysin2 induces clustering of phosphoinositides to recruit its downstream partner dynamin. *Nature Communications* **5**:5647. DOI: <https://doi.org/10.1038/ncomms6647>, PMID: 25487648
- Reiman EM**, Quiroz YT, Fleisher AS, Chen K, Velez-Pardo C, Jimenez-Del-Rio M, Fagan AM, Shah AR, Alvarez S, Arbelaez A, Giraldo M, Acosta-Baena N, Sperling RA, Dickerson B, Stern CE, Tirado V, Munoz C, Reiman RA, Huentelman MJ, Alexander GE, et al. 2012. Brain imaging and fluid biomarker analysis in young adults at genetic risk for autosomal dominant Alzheimer's disease in the presenilin 1 E280A kindred: a case-control study. *The Lancet Neurology* **11**:1048–1056. DOI: [https://doi.org/10.1016/S1474-4422\(12\)70228-4](https://doi.org/10.1016/S1474-4422(12)70228-4), PMID: 23137948
- Reitz C**, Jun G, Naj A, Rajbhandary R, Vardarajan BN, Wang LS, Valladares O, Lin CF, Larson EB, Graff-Radford NR, Evans D, De Jager PL, Crane PK, Buxbaum JD, Murrell JR, Raj T, Ertekin-Taner N, Logue M, Baldwin CT, Green RC, et al. 2013. Variants in the ATP-binding cassette transporter (ABCA7), apolipoprotein E ε4, and the risk of late-onset alzheimer disease in african americans. *Jama* **309**:1483–1492. DOI: <https://doi.org/10.1001/jama.2013.2973>, PMID: 23571587
- Rezazadeh M**, Khorrami A, Yeghaneh T, Talebi M, Kiani SJ, Heshmati Y, Gharesouran J. 2016. Genetic factors affecting Late-Onset Alzheimer's Disease Susceptibility. *NeuroMolecular Medicine* **18**:37–49. DOI: <https://doi.org/10.1007/s12017-015-8376-4>, PMID: 26553058
- Roberson ED**, Scearce-Levie K, Palop JJ, Yan F, Cheng IH, Wu T, Gerstein H, Yu GQ, Mucke L. 2007. Reducing endogenous tau ameliorates amyloid beta-induced deficits in an Alzheimer's disease mouse model. *Science* **316**:750–754. DOI: <https://doi.org/10.1126/science.1141736>, PMID: 17478722
- Roberson ED**, Halabisky B, Yoo JW, Yao J, Chin J, Yan F, Wu T, Hamto P, Devidze N, Yu GQ, Palop JJ, Noebels JL, Mucke L. 2011. Amyloid-β/Fyn-induced synaptic, network, and cognitive impairments depend on tau levels in multiple mouse models of Alzheimer's disease. *Journal of Neuroscience* **31**:700–711. DOI: <https://doi.org/10.1523/JNEUROSCI.4152-10.2011>, PMID: 21228179
- Rush T**, Roth JR, Thompson SJ, Aldaher AR, Cochran JN, Roberson ED. 2020. A peptide inhibitor of Tau-SH3 interactions ameliorates amyloid-β toxicity. *Neurobiology of Disease* **134**:104668. DOI: <https://doi.org/10.1016/j.nbd.2019.104668>, PMID: 31698056
- Sartori M**, Mendes T, Desai S, Lasorsa A, Herledan A, Malmanche N, Mäkinen P, Marttinen M, Malki I, Chapuis J, Flaig A, Vreulx AC, Ciancia M, Amouyel P, Leroux F, Déprez B, Cantrelle FX, Maréchal D, Pradier L, Hiltunen M, et al. 2019. BIN1 recovers tauopathy-induced long-term memory deficits in mice and interacts with tau through Thr<sup>348</sup> phosphorylation. *Acta Neuropathologica* **138**:631–652. DOI: <https://doi.org/10.1007/s00401-019-02017-9>, PMID: 31065832
- Savell KE**, Zipperly ME, Tuscher JJ, Duke CG, Phillips RA, Bauman AJ, Thukral S, Sultan FA, Goska NA, Ianov L, Day JJ. 2019a. A dopamine-induced gene expression signature regulates neuronal function and cocaine response. *bioRxiv*. DOI: <https://doi.org/10.1101/781872>
- Savell KE**, Bach SV, Zipperly ME, Revanna JS, Goska NA, Tuscher JJ, Duke CG, Sultan FA, Burke JN, Williams D, Ianov L, Day JJ. 2019b. A Neuron-Optimized CRISPR/dCas9 activation system for robust and specific gene regulation. *Eneuro* **6**:ENEURO.0495-18.2019. DOI: <https://doi.org/10.1523/ENEURO.0495-18.2019>, PMID: 30863790
- Scarmeas N**, Honig LS, Choi H, Cantero J, Brandt J, Blacker D, Albert M, Amati JC, Marder K, Bell K, Hauser WA, Stern Y. 2009. Seizures in alzheimer disease: who, when, and how common? *Archives of Neurology* **66**: 992–997. DOI: <https://doi.org/10.1001/archneurol.2009.130>, PMID: 19667221
- Seshadri S**, Fitzpatrick AL, Ikram MA, DeStefano AL, Gudnason V, Boada M, Bis JC, Smith AV, Carassquillo MM, Lambert JC, Harold D, Schrijvers EM, Ramirez-Lorca R, Debette S, Longstreth WT, Janssens AC, Pankratz VS, Dartigues JF, Hollingworth P, Aspelund T, et al. 2010. Genome-wide analysis of genetic loci associated with alzheimer disease. *Jama* **303**:1832–1840. DOI: <https://doi.org/10.1001/jama.2010.574>, PMID: 20460622
- Sottejeau Y**, Bretteville A, Cantrelle FX, Malmanche N, Demiaute F, Mendes T, Delay C, Alves Dos Alves H, Flaig A, Davies P, Dourlen P, Dermaut B, Laporte J, Amouyel P, Lippens G, Chapuis J, Landrieu I, Lambert JC. 2015. Tau phosphorylation regulates the interaction between BIN1's SH3 domain and Tau's proline-rich domain. *Acta Neuropathologica Communications* **3**:58. DOI: <https://doi.org/10.1186/s40478-015-0237-8>, PMID: 26395440
- St Martin JL**, Klucken J, Outeiro TF, Nguyen P, Keller-McGandy C, Cantuti-Castelvetri I, Grammatopoulos TN, Standaert DG, Hyman BT, McLean PJ. 2007. Dopaminergic neuron loss and up-regulation of chaperone protein mRNA induced by targeted over-expression of alpha-synuclein in mouse substantia nigra. *Journal of Neurochemistry* **100**:1449–1457. DOI: <https://doi.org/10.1111/j.1471-4159.2006.04310.x>, PMID: 17241127
- Tjondroesoemo A**, Park KH, Ferrante C, Komazaki S, Lesniak S, Brotto M, Ko JK, Zhou J, Weisleder N, Ma J. 2011. Disrupted membrane structure and intracellular Ca<sup>2+</sup> signaling in adult skeletal muscle with acute knockdown of Bin1. *PLOS ONE* **6**:e25740. DOI: <https://doi.org/10.1371/journal.pone.0025740>, PMID: 21984944
- Vossel KA**, Beagle AJ, Rabinovici GD, Shu H, Lee SE, Naasan G, Hegde M, Cornes SB, Henry ML, Nelson AB, Seeley WW, Geschwind MD, Gorno-Tempini ML, Shih T, Kirsch HE, Garcia PA, Miller BL, Mucke L. 2013. Seizures and epileptiform activity in the early stages of alzheimer disease. *JAMA Neurology* **70**:1158–1166. DOI: <https://doi.org/10.1001/jamaneurol.2013.136>, PMID: 23835471



- Vossel KA**, Ranasinghe KG, Beagle AJ, Mizuiri D, Honma SM, Dowling AF, Darwish SM, Van Berlo V, Barnes DE, Mantle M, Karydas AM, Coppola G, Roberson ED, Miller BL, Garcia PA, Kirsch HE, Mucke L, Nagarajan SS. 2016. Incidence and impact of subclinical epileptiform activity in Alzheimer's disease. *Annals of Neurology* **80**: 858–870. DOI: <https://doi.org/10.1002/ana.24794>, PMID: 27696483
- Wang HZ**, Bi R, Hu QX, Xiang Q, Zhang C, Zhang DF, Zhang W, Ma X, Guo W, Deng W, Zhao L, Ni P, Li M, Fang Y, Li T, Yao YG. 2016. Validating GWAS-Identified risk loci for Alzheimer's Disease in Han Chinese Populations. *Molecular Neurobiology* **53**:379–390. DOI: <https://doi.org/10.1007/s12035-014-9015-z>, PMID: 25452228
- Wijsman EM**, Pankratz ND, Choi Y, Rothstein JH, Faber KM, Cheng R, Lee JH, Bird TD, Bennett DA, Diaz-Arrastia R, Goate AM, Farlow M, Ghetti B, Sweet RA, Foroud TM, Mayeux R, NIA-LOAD/NCRAD Family Study Group. 2011. Genome-wide association of familial late-onset Alzheimer's disease replicates *BIN1* and *CLU* and nominates *CUGBP2* in interaction with *APOE*. *PLOS Genetics* **7**:e1001308. DOI: <https://doi.org/10.1371/journal.pgen.1001308>, PMID: 21379329
- Yu L**, Chibnik LB, Srivastava GP, Pochet N, Yang J, Xu J, Kozubek J, Obholzer N, Leurgans SE, Schneider JA, Meissner A, De Jager PL, Bennett DA. 2015. Association of brain DNA methylation in *SORL1*, *ABCA7*, *HLA-DRB5*, *SLC24A4*, and *BIN1* with pathological diagnosis of Alzheimer disease. *JAMA Neurology* **72**:15–24. DOI: <https://doi.org/10.1001/jamaneurol.2014.3049>, PMID: 25365775
- Zhang X**, Yu JT, Li J, Wang C, Tan L, Liu B, Jiang T. 2015. Bridging integrator 1 (BIN1) Genotype effects on working memory, hippocampal volume, and functional connectivity in young healthy individuals. *Neuropsychopharmacology* **40**:1794–1803. DOI: <https://doi.org/10.1038/npp.2015.30>, PMID: 25630570
- Zhou Y**, Hayashi I, Wong J, Tugusheva K, Renger JJ, Zerbinatti C. 2014. Intracellular clusterin interacts with brain isoforms of the bridging integrator 1 and with the microtubule-associated protein tau in Alzheimer's disease. *PLOS ONE* **9**:e103187. DOI: <https://doi.org/10.1371/journal.pone.0103187>, PMID: 25051234